PERFORMANCE EVALUATION OF DIAMOND TOOLS FOR MICRO-GROOVING

ANGSHUMAN GHOSH

(B.Sc. Engg.(Mech.), BUET)

A THESIS SUBMITTED

FOR THE DEGREE OF MASTER OF ENGINEERING

DEPARTMENT OF MECHANICAL ENGINEERING

NATIONAL UNIVERSITY OF SINGAPORE

2007

Acknowledgements

The author would like to express his deepest and heartfelt gratitude and appreciation to his supervisor Professor Mustafizur Rahman, Department of Mechanical Engineering, National University of Singapore (NUS), for his valuable guidance, continuous support and encouragement throughout the entire research work. It has been an honor for the author to work with Professor Rahman.

The author is greatly indebted to Mr. Neo Ken Soon, Professional Officer, Advanced Manufacturing Laboratory (AML), for his valuable suggestions and technical support. The author would also like to show his appreciation to Mr. Tan Choon Huat, Senior Laboratory Officer-In-Charge and Mr. Yeo Eng Huat (Nelson), Laboratory Officer, Advanced Manufacturing Laboratory (AML) for their technical assistance and support in performing the experimental works in the study. In this instance the author would like to appreciate Mr. Jamilon Bin Sukami, Final Year Project Student for sharing his time slot for the experiments.

At various stages of this research work, a lot of encouraging supports and help have come from the author's friends and colleagues which are heartily acknowledged with cordial thanks. Among them the author would like to specially thank Mr. K. V. R. Subrahmanyam, Mr. Woon Keng Soon, Mr. Shubhra Jyoti Bhadra, Mr. Md. Mazharul Haque, Mr. Ashim Kumar Debnath, Mr. Mohammad Ahsan Habib and Mr. Mohammad Majharul Islam.

The author would like to acknowledge the immense love and blessings, continuous inspiration and mental support throughout his life from his father – Mr. Arun Kiran Ghosh, mother – Mrs. Kalpona Ghosh and sister – Mrs. Modhumita Ghosh.

Finally the author would like to take this opportunity to show his sincere thank to National University of Singapore for the financial support and also for providing such a high-end research facility without which it would not be possible to conduct this research work.

Table of Contents

Acknowledgements i

Table of Contents iii

Summary vii

List of Tables ix

List of Figures x

List of Symbols xiv

Chapter One: Introduction 1

1.1 Overview & Motivation 1

1.2 Objectives 3

1.3 Organization of Thesis 3

Chapter Two: Literature Review 4

2.1 Introduction 4

2.2 Properties of Electroless Nickel Plating 5

2.2.1 Structure 5

2.2.2 Mechanical Properties 6

2.2.3 Hardness 7

2.2.4 Wear Resistance 7

2.2.5 Corrosion Resistance 8

2.3 Machining of Electroless Nickel 9

2.3.1 Machining with Diamond Tools 10

2.3.2 Diamond Tool Wear 12

2.3.3 Scope for Further Work 14

2.4 Conclusions 14

Chapter Three: Theoretical Aspects 16

3.1 Introduction 16

3.2 Chip Formation 16

3.3 Tool Geometry and Minimum Cutting Thickness 17

3.4 Cutting Force 22

3.5 Cutting Temperature 22

3.6 Cutting Fluid 22

3.7 Conclusions 23

Chapter Four: Experimental Details 24

4.1 Introduction 24

4.2 Experimental Set-up 24

4.2.1 Toshiba Ultra-Precision Machine 26

4.2.2 Diamond Tools 26

4.2.3 Workpiece 28

4.2.4 Force Data Acquisition System 30

4.2.5 Chip Removal System 30

4.2.6 Lubrication System 30

4.3 Measuring Equipments Used 31

4.3.1 Nomarski Optical Microscope 31

4.3.2 Keyence VHX Digital Microscope 31

4.3.3 JEOL JSM-5500 Scanning Electron Microscope 32

4.4 Experimental Procedure 33

4.4.1 Effect of Infeed Rate on Tool Life 35

4.4.2 Effect of Cutting Speed on Tool Life 36

4.4.3 Effect of Lubricant Material on Tool Life 37

4.4.4 Effect of Tool Point Angle on Tool Life 37

4.4.5 Tool Wear Observation 38

4.4.6 Machined Surface Observation 38

4.4.7 Chips Observation 39

4.5 Measurement and Data Analysis 39

4.5.1 Cutting Distance and Cutting Speed Measurement 39

4.5.2 Measurement of Tool Wear 40

4.5.3 Measurement of Micro-Cutting Force 40

4.6 Conclusions 41

Chapter Five: Results and Discussions 42

5.1 Introduction 42

5.2 Summary of the Experimental Results 43

5.2.1 Experiment Time 43

5.2.2 Fresh Tool Observation 45

5.3 Effects of Cutting Parameters on Tool Life 49

5.3.1 Effect of Infeed Rate on Tool Life 49

5.3.1.1 Effect of Infeed Rate on Tool Nose Wear 52

5.3.1.2 Effect of Infeed Rate on Cutting Force 54

5.3.2 Effect of Cutting Speed on Tool Life 57

5.3.2.1 Effect of Cutting Speed on Tool Nose Wear 59

5.3.2.2 Effect of Cutting Speed on Cutting Force 60

5.3.3 Effect of Lubricant Material on Tool Life 63

5.3.3.1 Effect of Lubricant Material on Tool Nose Wear 65

5.4 Performance Comparison between 45^0 and 60^0 Tools 67

5.5 Flank Wear 69

5.6 Machined Surface Observation 74

5.7 Chips Observation 76

5.8 Conclusions 79

Chapter Six: Conclusions and Recommendations 80

6.1 Introduction 80

6.2 Conclusions 80

6.3 Recommendations 82

Bibliography 83

List of Publication 87

Summary

Electroless-nickel which exhibits excellent properties such as hardness, corrosion resistance and wear resistance is generally used for molding dies of optical parts such as LCD. Diamond turning is commonly used to machine such dies to achieve high degree of surface finish and dimensional accuracy. However, the tool life in such machining is quite short, especially so in the machining of V-shape micro grooves. Tool wear in such application is a very important factor as small tool wear can lead to significant degradation of groove shape and hence reduce the service quality of the end products. While there have been some studies carried out for micro-grooving, no significant study has so far been carried out for very narrow angle grooves on cylindrical surface.

In this study, performance of single crystal diamond tools with tool point angles of 45^0 and 60^0 are evaluated. The wear criterion is set at 1.0μm nose wear for the cutting of 5.0μm deep V-grooves. In order to evaluate cutting performances, cutting parameters such as infeed rate, cutting speed and lubricant material were varied. In the early stage of the machining several chipped-off areas were observed at a distance from the cutting zone and they remained unchanged for rest of the experiment. However the microscopic observations of the tools during the experiments reveal that micro-grooves started forming and enlarging at the cutting zone on the flank faces with increasing cutting distance and eventually causing the tools to fail. Moreover chippings from the flank edge were observed during the machining. It was found experimentally that the 45^0 tools experienced catastrophic failure at the tool nose in the most cases whereas the 60^0 tools failed only once catastrophically. It was observed that the tools wore

gradually with cutting distance until they failed. From the experimental results, it is found that the 60^0 tools performed better than the 45^0 tools in terms of tool life based on complete groove cutting distance, the exception was when vegetable oil lubricant was used. In that case the 45^0 tool achieved higher tool life than the 60^0 tool. In addition the chips observations are the evidence of continuity of the chips and hence ensure the ductile mode cutting.

From the experimental results, it has been found that single crystal diamond tools can achieve the longest tool life based on complete groove cutting distance with cutting speed of 19.2m/min cutting speed and infeed rate of 2.0μm/rev. However no conclusive result has been found for selecting the lubricant material. It has also been observed that the 60^0 tool can perform better than the 45^0 tool in machining V-shape microgrooves.

List of Tables

Table-2.1: Physical and Mechanical Properties of Electroless Nickel-Phosphorus 6

Table-2.2: Taber Abraser Index for Wear Resistance of Electroless Nickel Plating..... 8

Table-4.1: Tool Configuration 27

Table-4.2: Cutting Parameter Matrix for Investigation of the Effect of Infeed Rate on Tool Life 36

Table-4.3: Cutting Parameter Matrix for Investigation of the Effect of Cutting Speed on Tool Life 36

Table-4.4: Cutting Parameter Matrix for Investigation of the Effect of Lubricant Material on Tool Life 37

Table-4.5: Cutting Parameter Matrix for Investigation of the Effect of Tool Point Angle on Tool Life..... 38

Table-5.1: Summary of the Experimental Results 44

List of Figures

Figure-3.1: Schematic of chip formation 17

Figure-3.2: A model of material behavior in diamond micro cutting 18

Figure-3.3: Differential cutting force in elastic region 18

Figure-3.4: Force model in cutting region 19

Figure-3.5: Stress on the stagnation point 20

Figure-4.1: Experimental Set-up 25

Figure-4.2: Toshiba Ultra-Precision Machine 26

Figure-4.3: Single Crystal Diamond Tool 27

Figure-4.4: Electroless Nickel Plated Workpiece, hollow end (4.4a), solid end (4.4b) 28

Figure-4.5: Schematic drawing of the machined workpiece 29

Figure-4.6(a): Schematic drawing of the 45^0 grooves (all dimensions in μm) 29

Figure-4.6(b): Schematic drawing of the 60^0 grooves (all dimensions in μm) 30

Figure-4.7: Nomarski Optical Microscope (OLYMPUS STM-6) 31

Figure-4.8: Keyence VHX Digital Microscope 32

Figure-4.9: JEOL JSM-5500 Scanning Electron Microscope 33

Figure-4.10: Schematic of Tool and Workpiece showing Cutting Force (F_c) and Thrust Force (F_t) 40

Figure-5.1: Microscopic views of the rake face of a fresh 45^0 tool (tool-5); 5.1(a) – Nomarski image and 5.1(b) – Keyence image 45

Figure-5.2: Microscopic views of the left flank face of a fresh 45^0 tool (tool-5); 5.2(a) – Nomarski image and 5.2(b) – Keyence image 46

Figure-5.3: Microscopic views of the right flank face of a fresh 45^0 tool (tool-5); 5.3(a) – Nomarski image and 5.3(b) – Keyence image 46

Figure-5.4: Microscopic views of the rake face of a fresh 60^0 tool (tool-8); 5.4(a) – Nomarski image and 5.4(b) – Keyence image 47

Figure-5.5: Microscopic views of the left flank face of a fresh 60^0 tool (tool-8); 5.5(a) – Nomarski image and 5.5(b) – Keyence image 48

Figure-5.6: Microscopic views of the right flank face of a fresh 60^0 tool (tool-8); 5.6(a) – Nomarski image and 5.6(b) – Keyence image 48

Figure-5.7(a): Effect of Infeed Rate on Tool Wear Progression for 45^0 Tools 50

Figure-5.7(b): Effect of Infeed Rate on Tool Wear Progression for 60^0 Tools 50

Figure-5.8(a): Effect of Infeed Rate on Tool Life for 45^0 Tools 51

Figure-5.8(b): Effect of Infeed Rate on Tool Life for 60^0 Tools 51

Figure-5.9: Catastrophic failure of tool nose for a 45^0 tool (tool-3, rake face); 5.9a-Nomarski image and 5.9b- Keyence image 53

Figure-5.10: SEM image of catastrophic failure of a 45^0 tool (tool-3) 53

Figure-5.11: Gradual progression of tool wear for a 60^0 tool (tool-14, rake face); 5.11a-Nomarski image and 5.11b- Keyence image 54

Figure-5.12(a): Effect of Infeed Rate on Cutting Force (F_c) for 45^0 Tools 54

Figure-5.12(b): Effect of Infeed Rate on Cutting Force (F_c) for 60^0 Tools 554

Figure-5.13(a): Effect of Infeed Rate on Thrust Force (F_t) for 45^0 Tools 55

Figure-5.13(b): Effect of Infeed Rate on Thrust Force (F_t) for 60^0 Tools 55

Figure-5.14(a): Effect of Infeed Rate on F_c/F_t for 45^0 Tools 56

Figure-5.14(b): Effect of Infeed Rate on F_c/F_t for 60^0 Tools 56

Figure-5.15(a): Effect of Cutting Speed on Tool Wear Progression for 45^0 Tools 57

Figure-5.15(b): Effect of Cutting Speed on Tool Wear Progression for 60^0 Tools 57

Figure-5.16(a): Effect of Cutting Speed on Tool Life for 45^0 Tools 58

Figure-5.16(b): Effect of Cutting Speed on Tool Life for 60^0 Tools 58

Figure-5.17: Catastrophic failure of tool nose for a 45^0 tool (tool-5, rake face); 5.17a-Nomarski image and 5.17b- Keyence image 60

Figure-5.18: Catastrophic failure of tool nose for a 60^0 tool (tool-13, rake face); 5.18a-Nomarski image and 5.18b- Keyence image 60

Figure-5.19(a): Effect of Cutting Speed on Cutting Force (F_c) for 45^0 Tools 61

Figure-5.19(b): Effect of Cutting Speed on Cutting Force (F_c) for 60^0 Tools 61

Figure 5.20(a): Effect of Cutting Speed on Thrust Force (F_t) for 45^0 Tools 62

Figure 5.20(b): Effect of Cutting Speed on Thrust Force (F_t) for 60^0 Tools 62

Figure 5.21(a): Effect of Cutting Speed on F_c/F_t for 45^0 Tools 62

Figure 5.21(b): Effect of Cutting Speed on F_c/F_t for 60^0 Tools 63

Figure-5.22(a): Effect of Lubricant Material on Tool Wear Progression for 45^0 tools 64

Figure-5.22(b): Effect of Lubricant Material on Tool Wear Progression for 60^0 tools 64

Figure-5.23(a): Effect of Lubricant Material on Tool Life for 45^0 Tools 65

Figure-5.23(b): Effect of Lubricant Material on Tool Life for 60^0 Tools 65

Figure-5.24: Gradual progression of tool wear for a 45^0 tool (tool-11, rake face); 5.24a- Nomarski image and 5.24b- Keyence image 66

Figure-5.25: Gradual progression of tool wear for a 60^0 tool (tool-15, rake face); 5.25a- Nomarski image and 5.25b- Keyence image 66

Figure-5.26: Performance Comparison between 45^0 and 60^0 Tools (Variation of Infeed Rate) 67

Figure-5.27: Performance Comparison between 45^0 and 60^0 Tools (Variation of Cutting Speed) 68

Figure-5.28: Performance Comparison between 45^0 and 60^0 Tools (Variation of Lubricant Material) 69

Figure-5.29: Nomarski image of grooves on left flank face of a 60^0 tool (tool-15); 5.29a- after 125m and 5.29b- after 536m cutting distance 70

Figure-5.30: Nomarski image of grooves on left flank face of a 45^0 tool (tool-3); 5.30a- after 176m and 5.30b- after 330m cutting distance 70

Figure-5.31: Keyence image of grooves on left flank face of a 45^0 tool (tool-3), after 279m cutting distance 71

Figure-5.32: SEM image of a 45^0 tool (tool-9) after 536m cutting distance 71

Figure-5.33: Keyence image of chipped-off area on left flank face of a 60^0 tool (tool-2), after 92m cutting distance 72

Figure-5.34: SEM image of a 60^0 tool (tool-2) after 811m cutting distance 73

Figure-5.35(a): Keyence image of chipped-off area on right flank face of a 60^0 tool (tool-8), after 484m cutting distance..... 73

Figure-5.35(b): Keyence image of chipped-off area on left flank face of a 60^0 tool (tool-8), after 484m cutting distance..... 74

Figure-5.36: Nomarski image of Machined Surface..... 75

Figure-5.37: 2-Dimensional Keyence image of Machined Surface..... 75

Figure-5.38: 3-Dimensional Keyence image of Machined Surface..... 76

Figure-5.39: SEM image of the cutting chips in machining of 1.6m to 11.9m cutting distance (X3000)..... 77

Figure-5.40: SEM image of the cutting chips in machining of 73.4m to 124.8m cutting distance (X1000)..... 77

Figure-5.41: SEM image of the cutting chips in machining of 124.8m to 176.1m cutting distance (X500)..... 78

Figure-5.42: SEM image of the cutting chips in machining of 124.8m to 176.1m cutting distance (X3000)..... 78

List of Symbols

B_c	Minimum cutting thickness
F_c	Cutting force
F_t	Thrust force
F_r	Resultant tool force
P_e	Normal stress on the round nose tool edge in elastic region
r	Tool edge radius
t_m	Minimum cutting thickness
w	Width of the tool
α	Tool rake angle
φ	Shear angle
β	Mean friction angle between the chip and the tool
β_e	Friction angle in elastic region
β_p	Friction angle in plastic angle
μ	Friction co-efficient
τ_s	Shear strength

Chapter One: Introduction

1.1 Overview & Motivation

Ultra precision machining is the term used for the process which can achieve a surface finish in the nanometer range. The need of producing parts of conventional dimensions with such surface finish led to evolution of this process from micromachining. In the 1970's, the ultra precision machining techniques were introduced for manufacturing of memory disks of the computer hard drives and also for photoreceptors components of photocopiers and printers where extremely high geometric accuracy and surface finish were required. This technique has resulted in lower overall manufacturing cost by rendering the multiple process of machining, lapping and finishing obsolete. Among the numerous applications of this technique, the manufacturing of optical parts with extremely high surface finish and geometric accuracy is the most effective one (Ikawa et al., 1991).

Ultra precision machining technique requires a synergy of the cutting parameters, workpiece and cutting tools. Diamond being the hardest of all materials is the most popular cutting tool for such technique. The Knoop indenters have revealed that the hardness value could vary between 56 and 102 GPa (equivalent to approximately 6000 to 10000 HV). The unique crystalline structure of diamond is the reason for its extreme hardness and this makes it possible to produce diamond tool with extraordinary sharp edges which are capable of generating surfaces of high degree of form accuracy and finish. However chipping of the edges of diamond tool due to its low toughness and the chemical interaction between diamond and ferrous materials restricts its use as a tool material in many cases (Trent and Wright, 2000).

Electroless-nickel is generally used as coatings for molding dies of plastic optical parts. Excellent physical and chemical properties like hardness, uniformity, corrosion resistance and wear resistance make it very suitable for such applications. Diamond turning has been successfully introduced to machine such types of dies without the need for post machining processes resulting in cost savings (Casstevens and Daugherty, 1978).

Several studies on machining such as face turning and face grooving of Electroless Nickel plated die materials with diamond tools and with different cutting parameters have been carried out. However no study has been carried out on machining V-shape micro-grooves with such narrow included angles of 45^0 and 60^0 on cylindrical dies. Such die has an increasing application in producing extremely high quality LCD (abbreviation of Liquid Crystal Display) by replicating those grooves on the substrate. Therefore, extremely high dimensional accuracy and surface finish of the micro-grooves on the die is a must. Tool life is a very important issue for such applications as a single cutter is usually required to machine a die in one set-up. However, tool life tends to be very short due to the inherent weakness of the narrow angle cutters and that a very small tool wear can only be tolerated. Hence all these have drawn attention to the investigations of the effects of various cutting parameters such as infeed rate, cutting speed and lubricant material on the performances of single crystal diamond tools with different tool point angles in this particular type of machining of electroless nickel plated die materials.

1.2 Objectives

In this study, investigations are carried out in the machining of V-shape micro-grooves on Electroless Nickel plated cylindrical dies using very narrow angle single crystal diamond tools of 45^0 and 60^0. The wear criterion is set at 1.0μm of nose wear for the cutting of 5.0μm deep V-grooves. The objectives of the study include the followings.

1. To investigate the effects of cutting parameters such as infeed rate, cutting speed and lubricant material on tool life.
2. To compare the performances of 45^0 and 60^0 diamond tools in such machining.
3. To investigate the wear characteristics of the diamond tools for this particular type of machining.
4. To investigate the machined surface and the chips produced during the cutting of V-grooves.

1.3 Organization of Thesis

A brief history of the Electroless Nickel Plating and pertinent diamond machining are discussed in the Chapter 2. The theoretical aspects of the microgrooving on brittle materials and the factors governing the process are described in the Chapter 3. Chapter 4 provides the details of experiments. A comprehensive discussion on the experimental results is presented in the Chapter 5. Chapter 6 leads to the concluding remarks from this study and also to the recommendations made for the future work.

Chapter Two: Literature Review

2.1 Introduction

Electroless nickel plating is an unusual engineering coating with unique properties and is used in many industrial applications. This particular plating exhibits excellent corrosion and wear resistance along with exceptional uniformity, solderability and brazability (Baudrand, 1978). These properties have made it possible to use this plating for many applications including those in petroleum, chemicals, plastics, optics, printing, mining, aerospace, nuclear, automotive, electronics, computers, textiles, paper, and food machinery (Parker, 1972). Moreover this plating can be applied on a wide range of substrates, conductive or nonconductive, because it does not require electrical current to be produced. The deposition process of the electroless nickel plating is an autocatalytic chemical reduction where nickel ions are reduced from an aqueous solution onto a catalytic surface (Casstevens and Daugherty, 1978).

Three different types of electroless nickel plating are produced; they are nickel-phosphorus (6 to 12% P), nickel-boron (~ 5% B), and composite coatings (combination of nickel-phosphorus and silicon carbide, fluorocarbons, or diamond particles). However the most widely used one is the nickel-phosphorus which has advantages over the other two including lower cost, greater ease of control of the deposition process, and better corrosion resistance of the deposit. The commercial electroless nickel-phosphorus is mostly deposited using Sodium Hypophosphite baths (Davis et al., 2000). These deposits do not require any heavy metal or sulphur-coating stabilizer and form a glassy, amorphous structure (Reidel, 1991).

Electroless nickel plating is machinable with diamond tools requiring no post-machining process. Several studies have been performed on machining of electroless nickel plating with diamond tools which are discussed later on this chapter. This chapter presents the properties of the electroless nickel-phosphorus plating and a brief review of the earlier machining of it with diamond tools.

2.2 Properties of Electroless Nickel Plating

Electroless nickel-phosphorus plating is uniform, hard, relatively brittle, lubricious, easily solderable, and highly corrosion and wear resistant. Its wear resistance is compared to that of commercial hard chromium coatings. Table 2.1 shows a summary of the properties of electroless nickel containing 10.5% P.

2.2.1 Structure

Electroless nickel-phosphorus is one of the very few metallic glasses used as an engineering material. The phosphorus content of it dominates their microstructure and the properties (Park and Lee, 1988). The structure of the as plated electroless nickel could be crystalline, amorphous, or a combination of both. However the commercial coatings containing 6 to 12% P dissolved in nickel and other impurities up to 0.25% are mostly amorphous in their as plated condition. The lower phosphorus content leads to porous structure resulting in cracks and holes that separate the columns of amorphous material. This adversely affects the ductility and the corrosion resistance of the coatings (Davis et al., 2000).

Table-2.1: Physical and Mechanical Properties of Electroless Nickel-Phosphorus Deposits (Davis et al., 2000)

Property[a]	Electroless Nickel-Phosphorus[b]
Density, g/cm^3 (lb/in^3)	7.75 (2.8)
Melting Point, ^{0}C (^{0}F)	890 (1630)
Electrical resistivity, μΩ.cm	90
Thermal conductivity, W/m.K (cal/cm.s.^{0}C)	4 (0.01)
Coefficient of thermal expansion (22-100^{0}C, or 72-212^{0}F), μm/m.^{0}C (μin/in.^{0}F)	12 (6.7)
Magnetic properties	Nonmagnetic
Internal stress, MPa (ksi)	Nil
Tensile strength	700 (100)
Ductility, % elongation	1.0
Modulus of elasticity, GPa (10^6 psi)	200 (29)
As-deposited hardness, HV_{100}	500
Heat-treated hardness, 400^{0}C (750^{0}F) for 1 h, HV_{100}	1100
Coefficient of friction vs steel, lubricated	0.13
Wear resistance, as-depsoited, Taber mg/1000 cycles	18
Wear resistance, heat treated 400^{0}C (750^{0}F) for 1 h, Taber mg/1000 cycles	9

[a] Properties are for coatings in the as-deposited conditions unless noted
[b] Hydrophosphite-reduced electroless nickel containing approximately 10.5% P

2.2.2 Mechanical Properties

The diffraction pattern of the electroless nickel deposits are very similar to those of materials that are rapidly cooled from the liquid state and considered to be glasses. Therefore it is also termed as glasses and the mechanical properties of the electroless nickel plating resemble those of other glasses (Mallory and Hajdu, 1990). These coatings have high strength, limited ductility, and a high modulus of elasticity. The tensile strength and strain at failure increases with increasing phosphorus content. Moreover high- phosphorus and high-purity coatings have higher ductility compared to

low-phosphorus and impure coatings. Table 2.1 shows some typical mechanical properties for electroless nickel containing 10.5% P (Davis et al., 2000).

2.2.3 Hardness

Hardness is the most widely studied property of electroless nickel plating (Reidel, 1991). The phosphorus content and heat treatment dominate the hardness of the electroless nickel which are extremely important property for many applications and also determines the cutting tool materials and the values of cutting parameters. The hardness value of electroless nickel decreases with the increasing phosphorus content and the minimum value of hardness can be achieved at a high phosphorus content of 11% (Duncan, 1983). The micro-hardness of electroless nickel coatings is about 500 to 600 HV_{100} in their as deposited condition, which is approximately equal to 48 to 52 HRC and equivalent to many hardened alloy steel. A controlled heat treatment causes these alloys to age harden and a heat treatment at 400^0C for one hour can produce hardness values as high as 1100 HV_{100}, equal to most commercial hard chromium coatings (Davis et al., 2000).

2.2.4 Wear Resistance

The electroless nickel coatings have excellent resistance to wear and abrasion, both in the as-deposited and hardened condition due to their high hardness. Table 2.2 shows the Taber Abraser Index values for wear resistance of electroless nickel containing 9% phosphorus.

Table-2.2: Taber Abraser Index for Wear Resistance of Electroless Nickel Plating (Davis et al., 2000)

Coatings	Heat Treatment for 1 h		Taber Wear Index[a], mg/1000 cycles
	^{0}C	^{0}F	
Electroless Nickel[b]	None	None	17
	300	570	10
	500	930	6
	650	1200	4

[a] CS-10 abraser wheels, 1000g load, determined as average weight loss per 1000 cycles for total test of 6000 cycles
[b] Hypophosphite reduced electroless nickel containing approximately 9% P

2.2.5 Corrosion Resistance

Electroless nickel protects the substrate by sealing it off the environment thus acting as a barrier coating rather than as a sacrificial one. The amorphous nature and the passivity make it highly corrosion resistant, even better than pure nickel or chromium alloys. The electroless nickel coatings containing higher phosphorus have amorphous microstructure and this has better resistance to corrosive attack than equivalent polycrystalline materials due to the absence of grain or phase boundaries and also due to the presence of the glassy films which form on and passivate their surfaces. The resistance to corrosive attack in neutral and acidic environments increases with increasing phosphorus content, however in alkaline corrosive environment the reverse happens. In addition heat treated (hardened) coatings should not be used where the primary objective is to resist corrosion (Davis et al., 2000).

2.3 Machining of Electroless Nickel

Because of the unique physical and mechanical properties, electroless nickel plating is used for applications requiring a combination of wear and corrosion resistance. Now-a-days, it is used extensively in the electronics and optical industries. However being an extremely hard and somewhat brittle material which offers very little ductility during machining, electroless nickel is required to be machined in ductile mode in order to generate high quality optical surface. The ductile mode machining of brittle materials by ultra-precision diamond turning has made it possible to generate mirror-surfaces on brittle materials (Ikawa et al., 1991).

A number of works have been performed in order to understand the ductile mode machining of brittle materials. In 1986, Toh and McPherson observed plastically deformed chips in the machining of ceramic materials using a depth of cut less than 1.0μm, which indicates a very interesting fact that the ductile mode cutting of brittle materials is possible if the depth of cut is in mesoscale. After that several researchers also observed that plastically deformed chips in the machining of a wide range of materials including ceramics, glasses, semiconductor materials and crystals (Blackley and Scattergood, 1994; Fang and Venkatesh, 1998; Moriwaki et al., 1992). They all reported that there is a brittle-to-ductile transition in machining brittle materials when the depth of cut is set to a very small value (usually < 10μm). In addition the tool cutting edge plays an important role in ductile mode machining of brittle materials. Asai and Kobayashi (1990) reported that in order to get a mirror surface in ultra-precision machining the thickness of undeformed chip must be equal to or smaller than the tool cutting edge radius.

2.3.1 Machining with Diamond Tools

The first reported study of diamond turning on electroless nickel plating was conducted by Casstevens and Daugherty in 1978. The machining was performed on an electroless nickel plated disk of 102mm diameter at Oak Ridge Y-12 Plant with spindle speeds of 350 to 1000rpm, feed rates of 2.54 to 14.5μm/rev and round nose diamond tools with nose radii of 0.53, 1.60, 3.18 and 25.4mm. In that study along with the explanation of the electroless nickel plating process, optical applications and important metallurgical and mechanical properties were presented. However in spite of conducting a wide range of experiments with varying the types of plating, thickness of plating, types of substrates and heat treatment of the plating, the calculated surface finish for typical diamond turning parameters were not achieved. They reported that tool radius did not greatly affect the surface roughness of machined workpiece if the tool advance was equal to the tool radius to give the same theoretical finish. According to them, the tool life was as about to same as that obtained during machining of softer fcc metals such as copper and aluminum. However the surface finish of diamond machined electroless nickel had a different appearance compared to those of fcc metals even both materials were machined with the same speed and tool advance. Electroless nickel plated surface was characterized by very uniform and distinct tool marks whereas the copper surface was achieved much smoother. In addition heat treatment of diamond-turned electroless nickel in a vacuum furnace roughened the surface slightly, giving it an orange-peel appearance. Moreover the tool life was shortened in machining hardened electroless nickel resulting very good surface finish.

Dini (1981) mentioned the substantial advantages of electroless nickel coating for diamond turning applications in his research. He reported that the best diamond

turning results were found in machining electroless nickel coatings which was produced from acid solutions containing hypophosphite as the reducing agent. However the coatings produced from alkaline solutions showed some irregularity in results causing immediate breaking of the tool edges. The importance of the quality and the reliability of the electroless nickel coatings for the diamond machining was pointed out by Sanger and Dini in 1982. Later in 1985 Syn et al. studied the machinability of electroless nickel with respect to diamond tool wear. They reported machinability as a function of phosphorus content and heat treatment condition. In their experiments they used electroless nickel containing various percentages of phosphorus (1.8 - 13%) hardened at different temperatures (200, 400 and 600^0C). The best results in terms of surface finish were obtained in machining of electroless nickel containing 11% phosphorus and hardened at 200^0C. In the same year 1985, Taylor et al. presented the surface finish achieved during machining of hardened electroless nickel containing 1.8% to 13% phosphorus. They used single crystal diamond tools at Precision Engineering Research Lathe (PERL) for the machining. According to them, the best surface finish was found in machining electroless nickel containing 13% phosphorus and hardened at 200^0C which produced amorphous structure that enhanced the surface finish.

In 2003, Pramanik et al. studied the effects of various cutting parameters such as depth of cut, feed rate and spindle speed and also the effect of phosphorus content on the surface finish of machined electroless nickel plated workpiece and on the diamond tool wear during a long distance cutting of 200km. The machining was conducted on a Toshiba ULG-100 ultra precision lathe with round nose diamond tools of 2mm nose radius. They reported that depth of cut had no significant effect on surface roughness

whereas it increased with increasing feed rate and decreased with increasing phosphorus content. In 2004, Rahman et al. investigated the performance and the suitability of single crystal diamond tools for microgrooving on electroless nickel plated workpieces. They reported that machining of microgrooves up to 50km cutting distance without any significant tool wear was possible and the surface roughness had a range of 4-6nm Ra. Later in 2005, Biddut studied the tool wear for single crystal diamond tools with different rake angles in machining microgrooves on the face of electroless nickel plated workpieces. He reported that a proper selection of cutting parameters and diamond tool with 0^0 rake angle resulted to a surface finish of 3nm.

2.3.2 Diamond Tool Wear

There are several studies on the machinability of electroless nickel plated workpiece containing different percentages of phosphorus and heat treatment at different temperature. However, there are only a few studies that were performed on tool wear of diamond tools during machining of such workpieces.

Casstevens and Daugherty (1978) reported the same tool life for diamond tools during machining of electroless nickel plated workpiece and softer fcc materials such as copper and aluminum. However microscopic observation revealed slight wear for diamond tools during machining of electroless nickel. Syn et al. (1986) investigated the diamond tool wear along with the surface finish for machining of hardened (at 200^0C for 2 h) electroless nickel containing 13% phosphorus for a cutting distance of 21.34km. Two types of single crystal natural diamond tools with different infrared absorptions characteristics (an indication of diamond impurity and hardness) were used. They reported that the surface roughness increased rapidly up to first 0.3km

cutting distance, after that it increased gradually up to 21.34km. The round nose tool tip was flattened due to tool wear resulting in burnishing rather than cutting of workpiece. According to them both the micro-fractures and the chemical reactions contributed to the wear of the tool edge causing grooves on flank face. The diamond tools having high hardness and lower fracture toughness predicted by infrared absorption measurements wore at a lower rate up to first 15.24km cutting, but exhibited more micro fracture on the tool edge.

Oomen and Eisses (1992) reported the wear behavior of diamond tools, for both natural and synthetic, determined by tool wear and cutting forces as a function of tool life. In machining of electroless nickel containing 9% phosphorus a wear pattern consisting of several grooves on the rake face known as crater wear along with some chipping off at the cutting edge was observed. However no significant difference in the wear pattern was observed for natural and synthetic diamond tools.

Pramanik et al. (2003) reported the wear characteristics of diamond tools for a very long distance cutting of electroless nickel containing different percentages of phosphorus. They also varied the cutting parameters such as depth of cut, feed rate and spindle speed. They observed no significant tool wear during the machining except for some defects on rake face after cutting of 15.6km. However very low tool wear occured on the flank face due to the repeated cutting up to 202km was reported. In 2004, Rahman et al. also reported no significant tool wear for machining microgrooves on electroless nickel plated workpiece up to a cutting distance of 50km. However after machining 28.5km some groove wears were observed on the rake face. Biddut (2005) conducted the evaluation of machining performance of the single crystal diamond tools

with different rake angles in face grooving of electroless nickel plated workpiece. He reported that there was no significant tool wear up to a cutting distance of 11.69km for diamond tools with 0^0 rake angle. However tool wear on rake and flank faces increased with the cutting distance for the diamond tools with $+5^0$ and -5^0 rake angles.

2.3.3 Scope for Further Work

So far several studies were performed on diamond turning and grooving on electroless nickel plated workpieces and also some studies on tool wear during such machining. However no study has been conducted on tool wear during machining of V-shape micro-grooves of such narrow included angles of 45^0 and 60^0 on electroless nickel plated cylindrical workpiece. Such machining is very important for industrial application of die production for LCD. So that it has become of immense importance to study the tool life of single crystal diamond tools with tool point angles of 45^0 and 60^0 as a function of tool wear in variation of the cutting parameters and also to study the wear characteristics.

2.4 Conclusions

Electroless nickel coatings have been long studied for a variety of industrial applications due to their unique physical and mechanical properties. A number of studies have been performed on the various factors affecting their properties. The effects of phosphorus contents and heat treatment on the machinability of electroless nickel coatings using diamond tools have been extensively studied. In addition some researchers studied the effects of cutting parameters on the machinability. It has been found that a hardened high phosphorus electroless nickel coating could be machined

using diamond tool resulting in extremely high degree of surface finish. However the tool wear being the most important factor affecting the surface finish has not been well studied especially in machining microgrooves on electroless nickel plated workpiece. So that it becomes very important to study the tool life of single crystal diamond tools as a function of tool wear for machining V-shape microgrooves of very narrow angles on electroless nickel plated cylindrical workpiece and also the corresponding effects of the cutting parameters on the tool life.

Chapter Three: Theoretical Aspects

3.1 Introduction

Ultra precision machining technique has a wide range of industrial applications including optical, aerospace and electronics industries due to the extremely high degree of dimensional accuracy and surface finish achievable. Therefore a clear understanding of the process is essential for its future development. In order to achieve the nano surface finish, it is required to machine brittle materials in ductile mode using this technique. This chapter focuses on some of the theoretical aspects governing ultra precision machining such as the chip formation, tool geometry and minimum cutting thickness, cutting force, cutting temperature and cutting fluid.

3.2 Chip Formation

The chip formation process can be described by the deformation of the workpiece material mostly in plastic regime due to the forces applied by the cutting tools on the workpiece. Figure 3.1 shows a schematic of chip formation during cutting. In the chip formation process the cutting tool removes a layer from the workpiece by deforming the uncut layer elastically first, then by deforming plastically near the cutting edge. This plastic deformation assumed to occur in a certain region entrapped between the undeformed materials and the edge of cutting tool (Bhattacharyya, 1984).

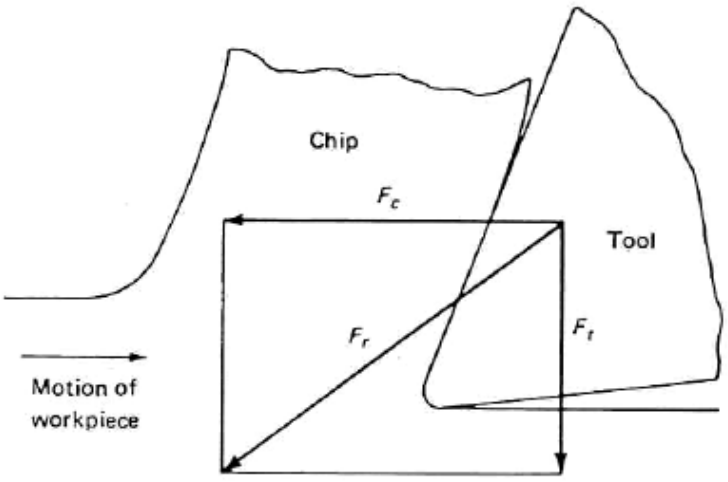

Figure-3.1: Schematic of chip formation (Boothroyd and Knight, 1989)

3.3 Tool Geometry and Minimum Cutting Thickness

The cutting mode is significantly affected by the tool geometry. Hence it is important to note that the sharpness of the diamond tool is the primary factor governing the cutting process and the quality of machined surface. Therefore, the cutting edge radius is the most important factor governing the brittle-to-ductile transition and this limits the minimum cutting thickness (Li et al., 2003). The minimum cutting thickness also depends on the physical relationship between the tool and the workpiece in ultra precision machining using diamond tool. The material behavior in precision diamond cutting in sub-micron range is shown in the figure 3.2. If the depth of cut is small compared to the tool edge radius, there may be some deformed but uncut materials underneath the tool. This phenomenon is termed as plowing and the force associated with this as plowing force. Although this force is irrelevant in macro cutting, it is very important factor in micro cutting.

In 2005, Son et al. proposed a cutting model for ultra precision diamond cutting involving the tool edge radius, minimum cutting thickness, cutting force and the

friction coefficient. According to them the workpiece is divided into perfectly plastic and perfectly elastic regions according to the minimum cutting thickness (B_c) as shown in figure 3.2.

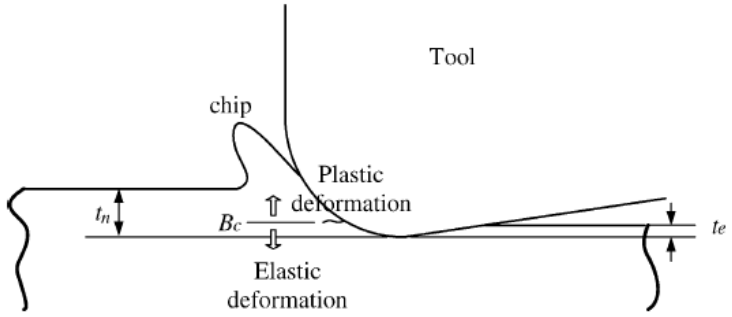

Figure-3.2: A model of material behavior in diamond micro cutting (Son et al., 2005)

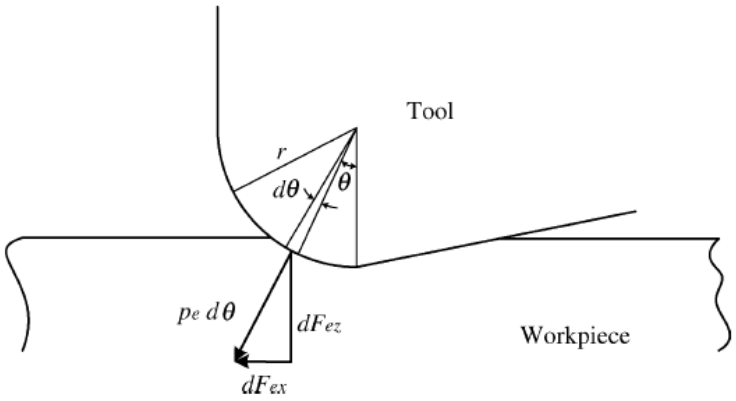

Figure-3.3: Differential cutting force in elastic region (Son et al., 2005)

The force relationship at a depth of cut of less than the minimum cutting thickness is shown in the figure 3.3. Since the workpiece is fully recovered after contact with a tool, the differential normal force and the differential tangential force could be expressed as the following equations.

$$\begin{aligned} dF_{ex} &= p_e r d\theta \sin\theta + \mu p_e r d\theta \cos\theta \\ dF_{ez} &= p_e r d\theta \cos\theta - \mu p_e r d\theta \sin\theta \end{aligned} \tag{3.1}$$

where, p_e is the normal stress on the rounded tool edge in the elastic region, r is the tool edge radius, and μ is the friction coefficient. The ratio dF_{ex}/dF_{ez} is given by,

$$\frac{dF_{ex}}{dF_{ez}} = \frac{p_e r d\theta \sqrt{(1+\mu^2)}\sin(\theta+\beta_e)}{p_e r d\theta \sqrt{(1+\mu^2)}\cos(\theta+\beta_e)} = \tan(\theta+\beta_e) \tag{3.2}$$

where, β_e is the friction angle in a perfectly elastic region.

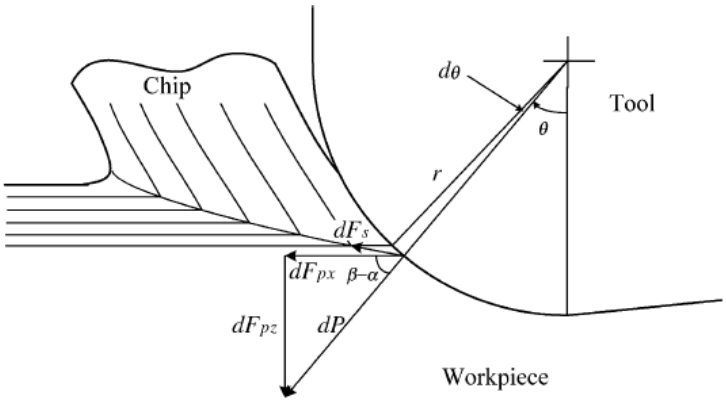

Figure-3.4: Force model in cutting region (Son et al., 2005)

The associated force model for the cutting depth more than perfectly elastic depth is shown in figure 3.4. The principle force using Merchant's force expression is given by,

$$dF_{px} = \frac{\tau_s w \cos(\beta_p - \alpha)}{\sin\phi\cos(\phi+\beta_p+\theta)} dt \tag{3.3}$$

where, τ_s is the shear strength, w is the width of the tool, β_p is the friction angle in a perfectly plastic region, α is the rake angle, and $dt = r\sin\theta d\theta$. Hence the principle force and the thrust force could be expressed as,

$$dF_{px} = \frac{-\tau_s w \sin\theta \sin(\beta_p + \theta)}{\sin\phi \sin(\phi + \beta_p + \theta)} d\theta \tag{3.4}$$

$$dF_{pz} = \frac{-\tau_s w \sin\theta \sin(\beta_p + \theta)}{\sin\phi \sin(\phi + \beta_p + \theta)} d\theta \tag{3.5}$$

From these two equations, the force relation could be written as,

$$\frac{dF_{ex}}{dF_{ez}} = \tan(\beta_e + \theta) \tag{3.6}$$

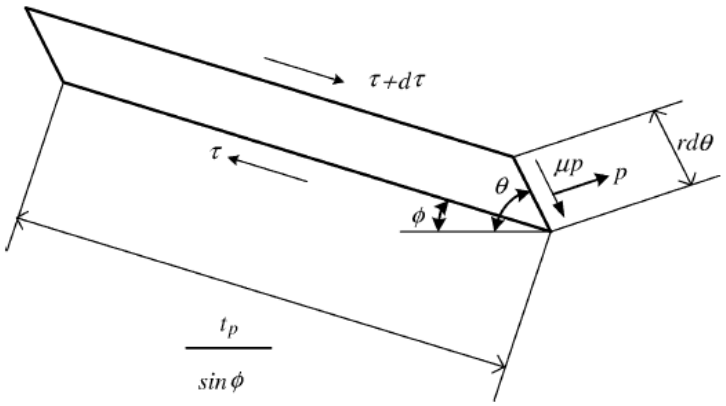

Figure-3.5: Stress on the stagnation point (Son et al., 2005)

Figure 3.5 shows all the stresses acting on a differential element under the minimum depth of cut. From the equilibrium of forces, an equation of the stagnation angle could be derived assuming the shear angle ϕ equal to the stagnation or neutral angle.

$$\frac{dF_{ex} / d\tau \, rd\theta \cos\theta_c}{dF_{ez} / d\tau \, rd\theta \sin\theta_c} = 1, \qquad \tan(\beta_e + \theta_c) = \cot\theta_c \tag{3.7a}$$

or,

$$\frac{dF_{ex}/d\tau \, rd\theta \cos\theta_c}{dF_{ez}/d\tau \, rd\theta \sin\theta_c} = 1, \qquad \tan(\beta_p + \theta_c) = \cot\theta_c \tag{3.7b}$$

Therefore, the minimum cutting thickness is given by,

$$t_m = r\left(1 - \cos\left(\frac{\pi}{4} - \frac{\beta}{2}\right)\right) \tag{3.8}$$

where,

t_m = minimum cutting thickness

r = cutting edge radius of the tool

β = either the friction angle between a tool and an uncut workpiece passed under the tool, β_e, or the friction angle between a tool and a continuous chip, β_p

It has been well reported that the tendency of generating sub-surface micro cracks in the brittle materials decreases with decrease in the undeformed chip thickness and almost disappear below a critical value of depth of cut. Moreover if the depth of cut is less than the cutting edge radius in the equation 3.8, the material is removed with the radius of the tool instead of rake face. The material under such conditions behaves in an elastic-plastic manner without fracture. However, it has been reported that at very shallow depth of cut with a blunt tool, the energy required to propagate cracks may be larger than the energy required for plastic yielding resulting the plasticity as the dominant material removal mechanism (Komanduri et al., 1998).

3.4 Cutting Force

It has been observed that the cutting force of ultra precision machining is usually at sub-Newton level. It is a very challenging task to measure such small force accurately since the force signal is significantly dominated by the noise generated from the mechanical and electrical sources and even from the earth. However the cutting force could explain the chip formation, tool wear and most importantly the cutting process.

3.5 Cutting Temperature

In diamond micro cutting, the temperature is quite low compared to that in conventional cutting because of low cutting energy as well as the high thermal conductivity of diamond (Ikawa et al., 1987). However, a very small temperature rise of the order of 10K in a tool may deteriorate the machining accuracy. Moreover according to Ikawa et al. (1991), the cutting temperature is one of the governing factors of the rate of diamond tool wear. On the other hand, hardness of the workpiece material decreases with the increasing temperature resulting in ductile mode cutting. So that it is of immense importance to conduct research on the cutting temperature and its effect on the diamond micro cutting.

3.6 Cutting Fluid

The cutting fluid for the ultra precision machining is applied to the cutting zone in a form of mist in order to improve the machining process. The cutting fluid can act as a coolant and/or as a lubricant. Moriwaki et al. (1990) reported that application of kerosene in a mist form in the cutting zone could reduce the temperature and machining error in ultra precision cutting of ductile material.

3.7 Conclusions

Various theoretical aspects such as chip formation, tool geometry and the minimum cutting thickness, cutting force, cutting temperature and cutting fluid governing the ultra precision machining using the diamond tool have been discussed. A clear understanding of their effects is essential for the development of the process.

Chapter Four: Experimental Details

4.1 Introduction

Electroless nickel, being a unique engineering coating for its outstanding properties of hardness, corrosion resistance and wear resistance, is generally used for molding dies of optical parts. In order to achieve high degree of dimensional accuracy and surface finish diamond turning has been successfully employed to machine electroless nickel. However the tool life of single crystal diamond tool in ultra-precision machining of electroless nickel plated die materials is very short especially in machining V-grooves of narrow included angles of 45^0 and 60^0 which are used for producing LCD. Therefore the main purpose of the present study is to evaluate the performances of the single crystal diamond tools with different tool point angles in machining V-shape micro-grooves on the electroless nickel plated cylindrical die materials. In order to evaluate the machining performances cutting parameters such as the infeed rate, the cutting speed and the lubricant material are varied. Plunge cut technique is applied in resulting intermittent cuttings to achieve the parallel grooves. This chapter aims to present the details of experimental set-up and the equipments used, to explain the experimental procedure and finally to describe how the measurement and the data analysis are performed.

4.2 Experimental Set-up

A Toshiba ULG-100 ultra-precision machine was used for the experiments. A photographic view of the experimental set-up is shown in the figure 4.1. It depicts the

position of vacuum chuck, workpiece, diamond tool, mist spray nozzle, chip suction nozzle and force dynamometer.

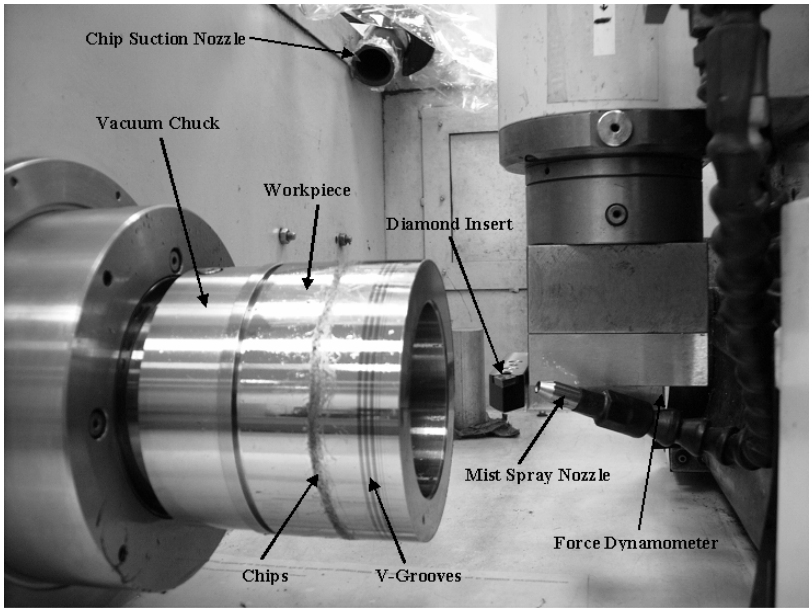

Figure-4.1: Experimental Set-up

The major components of the experimental set-up are as follows.

1. Toshiba Ultra-Precision Machine
2. Single Crystal Diamond Cutting Tool
3. Electroless Nickel Plated Workpiece
4. Cutting Force Data Acquisition System
5. Chip Removal System
6. Lubrication System

4.2.1 Toshiba Ultra-Precision Machine

In this study, a Toshiba ULG 100C (H^3) ultra-precision machine with a positioning resolution of 1 nm was used for the experiments. This machine is composed of an aerostatic bearing for work spindle, V-V rolling guideways with needle roller bearings and a FANUC 15 MB controller with 4 simultaneous controlled axes. Figure 4.2 show the two major units of this machine, namely the machining unit and the control unit.

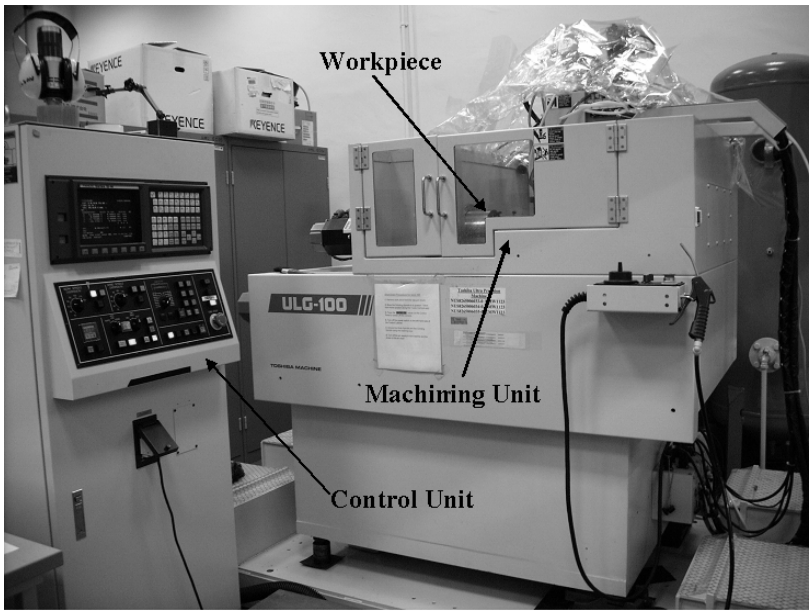

Figure-4.2: Toshiba Ultra-Precision Machine

4.2.2 Diamond Tools

Single crystal diamond tools of 45^0 and 60^0 tool point angles were used in this study. These artificial diamond tools were supplied by OSAKA Diamond of A.L.M.T. Corporation. These NewD type inserts are checked under 100X magnification before supplying and have cutting edge roughness of around 5μm. A total of 15 tools were used in this study. Table 4.1 shows the tool configurations. The tool number denotes

the number of the experiment where it was used. Figure 4.1 shows the photographic view of a tool used in this study.

Table-4.1: Tool Configuration

Tool Number	Tool Serial Number	Tool Point Angle	Crystallographic Orientation of Rake Face	Rake Angle	Front Clearance Angle	Tool Height, (mm)
1	EY43	$45^0$15’	{1 1 0}	$00^0$00’	$05^0$00	4.16
2	EY40	$60^0$00’	{1 1 0}	$00^0$00’	$03^0$50’	4.13
3	FB65	$44^0$40’	{1 1 0}	$00^0$00’	$05^0$00’	4.17
4	FB64	$44^0$40’	{1 1 0}	$00^0$00’	$05^0$00’	4.07
5	FB67	$44^0$45’	{1 1 0}	$00^0$00’	$05^0$00’	4.13
6	FB68	$44^0$45’	{1 1 0}	$00^0$00’	$05^0$00’	4.11
7	FB69	$44^0$40’	{1 1 0}	$00^0$00’	$05^0$10’	4.07
8	FF48	$60^0$05’	{1 1 0}	$00^0$00’	$03^0$00’	4.12
9	FJ72	$44^0$40’	{1 1 0}	$00^0$00’	$04^0$50’	4.16
10	FF49	$59^0$35’	{1 1 0}	$00^0$00’	$03^0$30’	4.17
11	FJ73	$44^0$50’	{1 1 0}	$00^0$00’	$04^0$50’	4.11
12	FF50	$59^0$50’	{1 1 0}	$00^0$00’	$03^0$55’	4.17
13	FF51	$60^0$00’	{1 1 0}	$00^0$00’	$04^0$15’	4.16
14	FF52	$60^0$00’	{1 1 0}	$00^0$00’	$04^0$30’	4.16
15	FF53	$60^0$06’	{1 1 0}	$00^0$00’	$04^0$30’	4.10

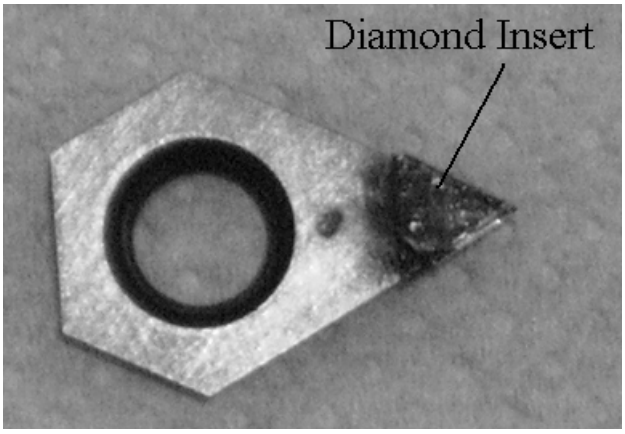

Figure-4.3: Single Crystal Diamond Tool

4.2.3 Workpiece

The workpiece material was electroless plated nickel of 100μm thickness on a hollow Starvax drum of 50mm length and 100mm diameter. The phosphorus content of the electroless nickel was 11.5% w/w. The blind hole was made in the base drum to reduce the weight. To achieve the perfectly flat surface on the solid end, it was trimmed before the experiment. After mounting the workpiece on the spindle with a vacuum chuck, each time the outside plating of electroless nickel was trimmed by a round nose diamond cutter to obtain perfect concentric plating. The photographs representing both the hollow end and the solid end of the workpiece are shown in the figure 4.4.

Figure-4.4(a)

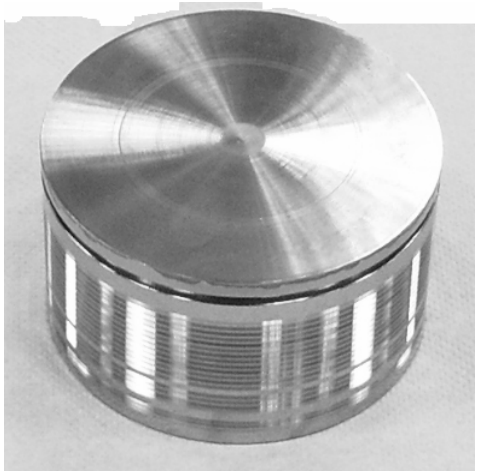

Figure-4.4(b)

Figure-4.4: Electroless Plated Nickel Workpiece, hollow end (4.4a), solid end (4.4b)

The V-shape micro-grooves on the machined surface of the workpiece are schematically shown in the figure 4.5.

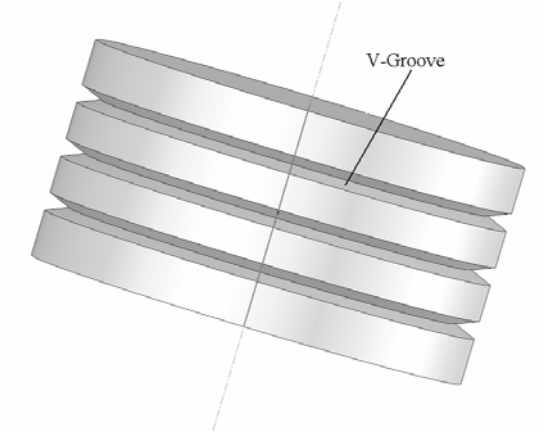

Figure-4.5: Schematic drawing of the machined workpiece

The micro-grooves with 45^0 and 60^0 included angles were machined on the workpiece. The depth of the grooves for each type was 5µm. The details of the micro-grooves of 45^0 and 60^0 included angles are shown in the figure 4.6(a) and figure 4.6(b) respectively.

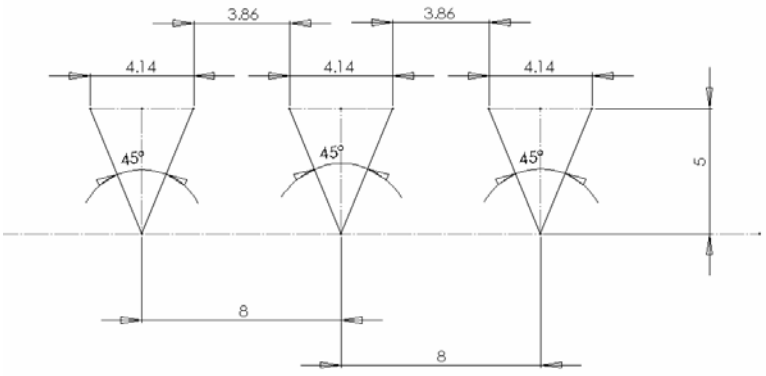

Figure-4.6(a): Schematic drawing of the 45^0 grooves (all dimensions in µm)

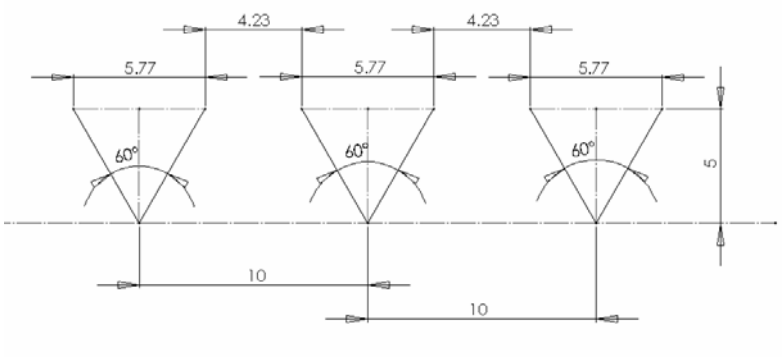

Figure-4.6(b): Schematic drawing of the 60^0 grooves (all dimensions in μm)

4.2.4 Force Data Acquisition System

A KISTLER (9256A) 3-Component dynamometer was used for measuring the micro-cutting forces. The signals of the cutting force F_c and thrust force F_t from the dynamometer were amplified by the KISTLER (Type 5015) charge amplifiers. In the same time a SONY digital data recorder (PC204Ax) recorded these signals into a SONY data cartridge of 2 GB capacity. These recorded digital data were later processed using PC Scan II data acquisition software.

4.2.5 Chip Removal System

The chip removal system was used to facilitate the removal of chips from the tool workpiece interface and to maintain clean cutting condition. This system consists of a compressor, a suction pipe and a suction nozzle.

4.2.6 Lubrication System

The mist lubrication was used in this study. The lubrication system contains a pump, lubricant container, a pipe and a spray nozzle. The flow of the lubricant material was kept constant throughout all the experiments.

4.3 Measuring Equipments Used

4.3.1 Nomarski Optical Microscope

A Nomarski Optical Microscope (OLYMPUS STM-6) was used to observe the tool condition at certain intervals. It was also used to observe the machined surface of the workpiece. There are two magnifications in this microscope, 100X and 500X. A digital camera and also a computer are connected to the microscope, which are used to capture and to record the images. Figure 4.7 shows the photograph of the Nomarski microscope used in this study.

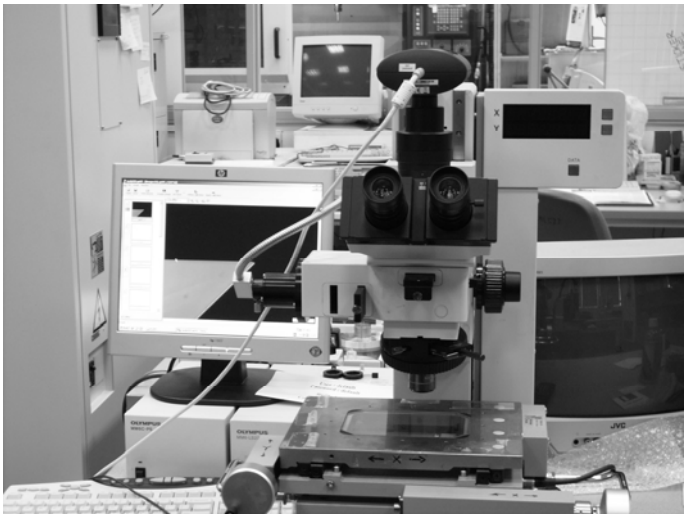

Figure-4.7: Nomarski Optical Microscope (OLYMPUS STM-6)

4.3.2 Keyence VHX Digital Microscope

A Keyence VHX Digital Microscope (figure 4.8) was used to observe the tool condition at certain intervals and the most importantly to measure the tool wear. It was also used to capture the 3-D view of the machined surface of the workpiece. The highest magnification achievable by this microscope is 3000X. This machine is

composed of two major units, a Color CCD camera with optical zoom lens and a monitor attached with a data processing unit.

Figure-4.8: Keyence VHX Digital Microscope

4.3.3 JEOL JSM-5500 Scanning Electron Microscope

After reaching the wear criterion, the diamond tools were observed using a JEOL JSM-5500 Scanning Electron Microscope (SEM). Unlike optical microscopes, it can show three faces (rake face, left and right flank faces) of the tool on a single image. It has a resolution of 3.5 nm. The maximum values of magnification and accelerating voltage achievable with this machine are respectively 50000X and 30KV. However in this study the tool observations were performed using 3000X magnification. The SEM used in this study is shown in the figure 4.9.

Figure-4.9: JEOL JSM-5500 Scanning Electron Microscope

4.4 Experimental Procedure

The experimental set-up shown in the figure 4.1 was used for all the experiments in this study. The workpiece was mounted on the spindle with a vacuum chuck and was balanced with a dial indicator. After mounting, the workpiece was trimmed by a round nose diamond cutter to obtain perfect concentric plating. A diamond cutter of 2mm nose radius, 500rpm spindle speed, 10mm/min feed rate, 3μm depth of cut and oil mist were used for this trimming. Depending upon the flatness of the plating, 9-27μm thickness of the plating was trimmed off each time. The machined workpiece was further trimmed for reusing until at least 10μm thickness of the plating remained on the Starvax drum for the safety reason. The diamond tool was screwed to the tool holder and the holder was screwed under the dynamometer.

The grooves were parallel to each other on the cylindrical workpiece (figure 4.5). So that plunge cut technique was applied resulting in intermittent cuttings to achieve those parallel grooves. In order to achieve a 5μm deep groove, 5 cutting passes were performed where each cutting pass involved a 1.0μm depth of cut (for 0.5 and

1.0μm/rev infeed rate). For 2.0μm/rev infeed rate, a 1.0μm depth of cut was used for all the grooves in first pass, and then a 2.0μm depth of cut was used for next two passes. In this study, a 1.0μm depth was cut in the first pass for each groove of a batch of certain grooves (for example 160 grooves), then in the next pass another 1.0μm (or 2.0μm) was cut for each groove and this process was repeated until the 5.0μm deep groove achieved.

The machining process can be divided into five major parts and they are-

1. Finding the effect of infeed rate on tool life
2. Determination of the effect of cutting speed on tool life
3. Investigating the effect of lubricating material on tool life
4. Checking the effect of tool point angle on the tool life
5. Observation of tool wear characteristics during the machining

The steps followed for all the experiments are as follows.

1. Mounting of the workpiece on the spindle and required trimming
2. Machining of 32 grooves (approx. 10m cutting distance)
3. Observation of the cutting tool with Nomarski and Keyence Microscopes
4. Machining of next 32 grooves (approx. 10m cutting distance)
5. Observation of the cutting tool with Nomarski and Keyence Microscopes
6. Machining of 160 grooves (approx. 50m cutting distance)
7. Observation of the cutting tool with Nomarski and Keyence Microscopes
8. Machining next 160 grooves and then tool observation until the tool reached the wear limit of 1.0μm nose wear
9. Observation of the worn tool with the Scanning Electron Microscope

A total of 15 experiments were performed for this study. Among them three experiments were ruled out because the tools failed in very early stage of the machining.

4.4.1 Effect of Infeed Rate on Tool Life

In order to investigate the effect of infeed rate on tool life, cutting speed was kept constant at 100rpm (approx. 32m/min) and a kerosene based mist (UP2T) was used as lubricant. A total of six experiments were performed, three experiments using three different infeed rates for each type of tool. Table 4.2 shows the cutting parameter matrix.

Table-4.2: Cutting Parameter Matrix for Investigation of the Effect of Infeed Rate on Tool Life

Number	Experiment Number	Tool Point Angle	Infeed Rate (μm/rev)	Cutting Speed (rpm, m/min)	Lubricant Material
1	1	45^0	0.5	100, 32	UP2T
2	3	45^0	1.0	100, 32	UP2T
3	4	45^0	2.0	100, 32	UP2T
4	2	60^0	0.5	100, 32	UP2T
5	13	60^0	1.0	100, 32	UP2T
6	14	60^0	2.0	100, 32	UP2T

4.4.2 Effect of Cutting Speed on Tool Life

To find the effect of cutting speed on tool life, infeed rate was kept constant at 1.0μm/rev and kerosene based mist (UP2T) was used as lubricant. A total of six experiments were performed for two types of diamond tool by varying three different cutting speeds of 100rpm (32m/min), 60rpm (19m/min) and 30rpm (10m/min),. The cutting parameter matrix is shown in table 4.3.

Table-4.3: Cutting Parameter Matrix for Investigation of the Effect of Cutting Speed on Tool Life

Number	Experiment Number	Tool Point Angle	Infeed Rate (μm/rev)	Cutting Speed (rpm, m/min)	Lubricant Material
1	3	45^0	1.0	100, 32	UP2T
2	5	45^0	1.0	60, 19	UP2T
3	9	45^0	1.0	30, 10	UP2T
4	13	60^0	1.0	100, 32	UP2T
5	8	60^0	1.0	60, 19	UP2T
6	10	60^0	1.0	30, 10	UP2T

4.4.3 Effect of Lubricant Material on Tool Life

In order to investigate the effect of lubricant material on tool life, infeed rate and cutting speed were kept constant at respectively 1.0μm/rev and 60rpm (approx. 19m/min). A kerosene based mist (UP2T) and a vegetable oil (Johnson's Baby Oil) were used as lubricant material. The cutting conditions are shown in table 4.4.

Table-4.4: Cutting Parameter Matrix for Investigation of the Effect of Lubricant Material on Tool Life

Number	Experiment Number	Tool Point Angle	Infeed Rate (μm/rev)	Cutting Speed (rpm, m/min)	Lubricant Material
1	5	45^0	1.0	60, 19	UP2T
2	11	45^0	1.0	60, 19	Vegetable Oil
3	8	60^0	1.0	60, 19	UP2T
4	15	60^0	1.0	60, 19	Vegetable Oil

4.4.4 Effect of Tool Point Angle on Tool Life

In this study, a total of 12 different experiments were done. Among them 6 experiments were done using 45^0 tools and the rest were performed using 60^0 tools. Here every set of cutting condition was used with both the tools. Table 4.5 shows the cutting parameter matrix used for this study.

Table-4.5: Cutting Parameter Matrix for Investigation of the Effect of Tool Point Angle on Tool Life

Number	Experiment Number	Tool Serial Number	Tool Point Angle	Infeed Rate (μm/rev)	Cutting Speed (rpm, m/min)	Lubricant Material
1	1	EY43	45^0	0.5	100, 32	UP2T
2	3	FB65	45^0	1.0	100, 32	UP2T
3	4	FB66	45^0	2.0	100, 32	UP2T
4	5	FB67	45^0	1.0	60, 19	UP2T
5	9	FJ72	45^0	1.0	30, 10	UP2T
6	11	FJ73	45^0	1.0	60, 19	Veg. Oil
7	2	EY40	60^0	0.5	100, 32	UP2T
8	13	FF51	60^0	1.0	100, 32	UP2T
9	14	FF52	60^0	2.0	100, 32	UP2T
10	8	FF48	60^0	1.0	60, 19	UP2T
11	10	FF49	60^0	1.0	30, 10	UP2T
12	15	FF53	60^0	1.0	60, 19	Veg. Oil

4.4.5 Tool Wear Observation

The fresh tools were observed using Nomarski and Keyence microscopes. Three faces of the tool, namely rake face, left flank face and right flank face were checked before the experiment. Then at certain intervals the tool was checked by Nomarski and Keyence Microscopes and the images were recorded. The tool wear was measured with the Keyence Microscope. Finally the worn tool was observed using the Scanning Electron Microscope after the experiment.

4.4.6 Machined Surface Observation

It was a challenging task to observe the machined surface, because the grooves were of very narrow angle and only 5μm deep. Moreover the working depth of the Keyence Microscope was smaller than the diameter of the workpiece. So that it was required to saw the workpiece into small pieces, to clean it properly and only then it could be

observed by the Nomarski and Keyence Microscopes. The Keyence microscope created 3-D view of the machined surface showing the V-grooves.

4.4.7 Chips Observation

Cutting chips were collected and then observed using the Scanning Electron Microscope. They were placed on a carbon tape to be observed by SEM.

4.5 Measurement and Data Analysis

4.5.1 Cutting Distance and Cutting Speed Measurement

In this study, cutting distances were calculated based on complete groove cutting length.

$$\text{Cutting Distance for 1 groove} = \pi \times \text{diameter of the workpiece} \quad (4.1)$$

Cutting speed in terms of spindle speed was first selected and then it was converted into m/min unit. The equation used for this was-

$$V = \pi \times d \times n \quad (4.2)$$

Where,

V = Cutting Speed in m/min

d = Diameter of the Workpiece in m

n = Spindle Speed in rpm

4.5.2 Measurement of Tool Wear

The tool wear was measured using the Keyence Microscope. At certain intervals the images of the three faces of the tool (rake and two flank faces) were taken by this machine and then the measurement was done using the attached data processing unit.

4.5.3 Measurement of Micro-Cutting Force

The two components of the micro-cutting forces, cutting force F_c and thrust force F_t were recorded during the machining (figure 4.10). These data were retrieved from the data cartridge using the SONY Digital Data Recorder through an interface and the PC Scan II software installed in the computer. The data were observed on real time plots and cutting zones were located. These cutting zone data were exported as PCscan II Binary Files (*.bin) to Matlab software. A Matlab program was then used to calculate the average value of a particular cutting zone force.

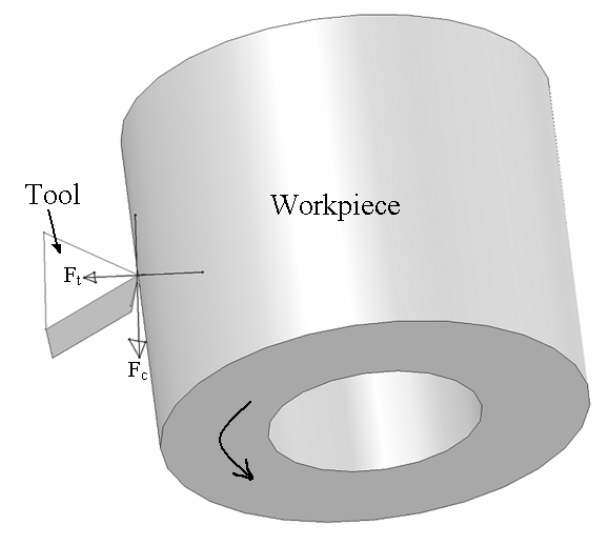

Figure-4.10: Schematic of Tool and Workpiece showing
Cutting Force (F_c) and Thrust Force (F_t)

4.6 Conclusions

In this chapter the experimental set-up, the equipments used and the details of the experimental procedure along with the measurement and data analysis technique for ultra-precision machining of electroless nickel plated die materials with diamond tools are discussed.

Chapter Five: Results and Discussions

5.1 Introduction

Ultra-precision machining is a remarkably important manufacturing technique in the electronics and aerospace industry. Moreover ultra-precision finishing of optical parts has become an exceedingly popular method to achieve high degree of surface finish. The process of the ultra-precision machining is not solely governed by the cutting parameters, but also significantly by cutting tool and workpiece materials. Diamond being the hardest material among all has been introduced successfully as the cutting tool for ultra-precision machining. Electroless-nickel which exhibits excellent properties such as hardness, corrosion resistance and wear resistance is generally used for molding dies of optical parts such as LCD. Diamond turning is commonly used to machine such dies. However, the tool life for such machining is quite short especially so in machining of V-shape micro grooves of very narrow included angles such as 45^0 and 60^0. So that it is of immense importance to evaluate the cutting performance and tool life of diamond cutter for that machining. This chapter aims to present the following results and discuss them.

- The effect of the different cutting parameters on tool life
- Performance comparison between 45^0 and 60^0 tools
- The wear characteristics of diamond tool
- Machined surface and cutting chips observations

5.2 Summary of the Experimental Results

In this study a total of 15 experiments were conducted. Among them 3 experiments were discarded, because the tools with initial subsurface fine cracks and rough edges failed in the very early stage of the machining. However those three experiments were conducted again with new tools and same cutting conditions as discarded experiments. Moreover the comparison of the results of discarded experiments with the repeated experiments further confirmed that in the previous cases the tools failed due to inherent cracks, not due to the cutting conditions. Finally there is a total of 12 experiments to be analyzed. The summary of the experimental results is shown in the table 5.1.

5.2.1 Experiment Time

In this study, intermittent cutting was applied to achieve the parallel grooves on the workpiece. Hence the actual tool-workpiece contact time was a small fraction of the total machining time. After each cutting pass of a groove, the tool was retracted for 10μm and then moved to the next position to cut the next groove. For the retracted position, the tool then approached the workpiece at the speed of the infeed rate. This approaching time was much higher than the cutting time and hence increased the total machining time. After machining a certain numbers of grooves (as mentioned in Chapter 4), i.e. a certain cutting distance, the tool was observed under Nomarski and Keyence Microscopes. Finally the tool was observed under SEM.

Table-5.1: Summary of the Experimental Results

No.	Expt. No.	Tool Point Angle (degree)	Work-piece Dia-meter (mm)	Infeed Rate (µm/rev)	Cutting Speed (rpm, m/min)	Lubricant Material	Tool Life (m)	Total No. of Grooves Cut	Total Cutting Distance (m)	Actual Tool-Workpiece Contact Time		Machining Time for A Complete Expt. (hrs:mins)	Expt. Time (days)
										For A Complete Groove (sec)	Total Time up to Tool Life (hrs:mins)		
1	1	45	102.1	0.5	100, 32.1	UP2T	182	879	282.2	12	1:53.48	16:6.9	6
2	3	45	102.1	1.0	100, 32.1	UP2T	288	1029	330.1	9	2:14.63	10:17.4	3
3	4	45	102.1	2.0	100, 32.1	UP2T	1101	3589	1151.4	5.4	5:8.92	12:33.69	6
4	5	45	102.1	1.0	60, 19.2	UP2T	706	2309	740.5	15	9:10.26	38:29	8
5	9	45	102.1	1.0	30, 9.6	UP2T	445	1669	535.7	30	11:33.67	55:38	8
6	11	45	102.1	1.0	60, 19.2	Vegetable Oil	1216	3909	1254.8	15	15:47.76	65:9	10
7	2	60	102.1	0.5	100, 32.1	UP2T	415	2528	811	12	4:18.76	25:48.8	9
8	13	60	102.1	1.0	100, 32.1	UP2T	302	1029	330.3	9	2:21.23	10:17.4	2
9	14	60	102.1	2.0	100, 32.1	UP2T	1277	4069	1306.1	5.4	5:58.3	14:14.49	5
10	8	60	102.1	1.0	60, 19.2	UP2T	901	3269	1049.3	15	11:42.25	54:29	11
11	10	60	102.1	1.0	30, 9.6	UP2T	767	2469	792.5	30	19:55.61	82:18	10
12	15	60	102.1	1.0	60, 19.2	Vegetable Oil	465	1669	535.7	15	6:2.42	27:49	5

5.2.2 Fresh Tool Observation

Prior to the start of each experiment the tool was checked under the Nomarski and Keyence microscopes. The tool was observed for any initial wear on tool nose or the flank edges. Three faces namely rake face, left flank face and right flank face were checked with the both microscopes. It was observed that the 60^0 tools came with a better finish whereas there were some initial wear marks on flank edges for the 45^0 tools. These tools are hand finished and it is very difficult to finish the tools very perfectly especially for such narrow angle of 45^0. Figures 5.1 shows respectively the Nomarski and the Keyence images of the rake face of a fresh 45^0 tool which was used in the experiment-5.

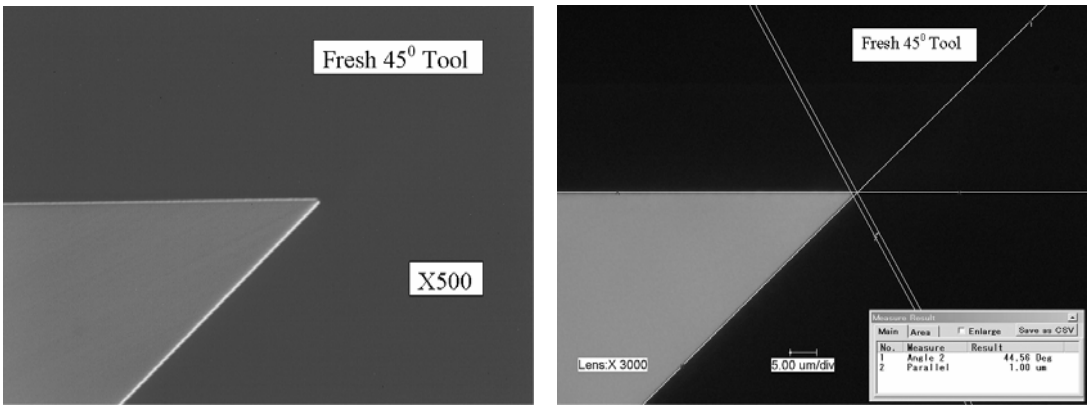

Figure-5.1(a) Figure-5.1(b)

Figure-5.1: Microscopic views of the rake face of a fresh 45^0 tool (tool-5); 5.1(a) - Nomarski image and 5.1(b) - Keyence image

The bright straight lines on the cutting edges (figure-5.1a) confirmed that this tool had no initial wear marks on the cutting edges of rake face. From figure 5.1b it could be seen that this tool was initially worn up to 1μm of tool nose. So that the progressive tool wear was calculated by setting this value as a reference. Each and every tool's rake face was checked in the similar fashion.

Figures 5.2a and 5.2b show the Nomarski and Keyence images of the left flank face of the same tool respectively. They are the evidence that flank edge was not perfectly sharp for this tool. Most 45^0 tools used in this study exhibited this feature. The bright straight line in the figure 5.2a represents the perfectly sharp and straight cutting edge of rake face. The Nomarski and Keyence images of the right flank face of the same tool are shown in the figures 5.3a and 5.3b. From these two images the initial wear marks on the flank edge could be seen.

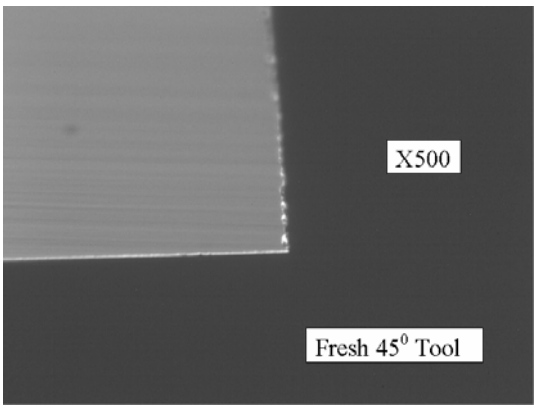

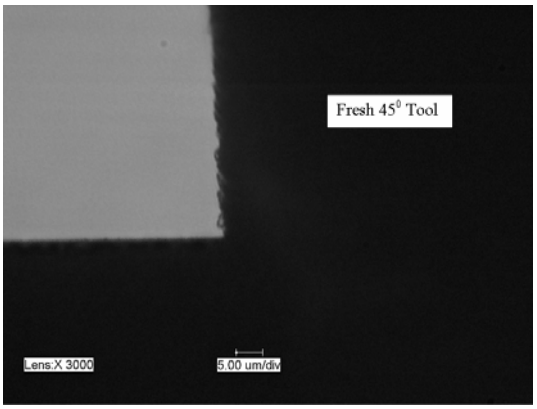

Figure-5.2(a) Figure-5.2(b)

Figure-5.2: Microscopic views of the left flank face of a fresh 45^0 tool (tool-5); 5.2(a) - Nomarski image and 5.2(b) - Keyence image

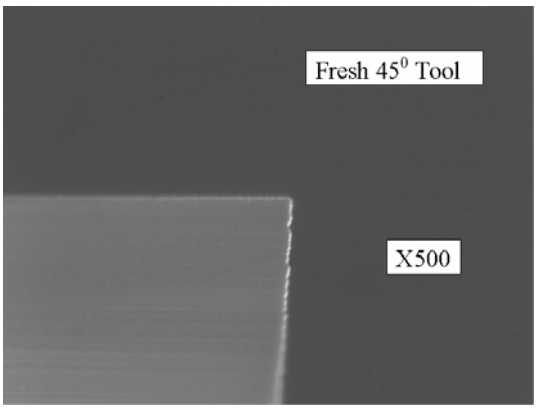

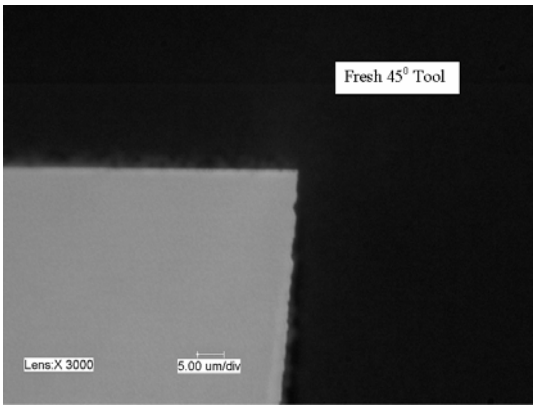

Figure-5.3(a) Figure-5.3(b)

Figure-5.3: Microscopic views of the right flank face of a fresh 45^0 tool (tool-5); 5.3(a) - Nomarski image and 5.3(b) - Keyence image

Figures 5.4a and 5.4b represent the Nomarski and Keyence images of the rake of a 60^0 tool used in the experiment-8. This tool had perfectly sharp and straight cutting edge on rake face as confirmed by the bright straight lines on the cutting edge (figure 5.4a). However it had an initial nose wear of 0.70μm. The progressive tool wear was measured with respect to this initial nose wear.

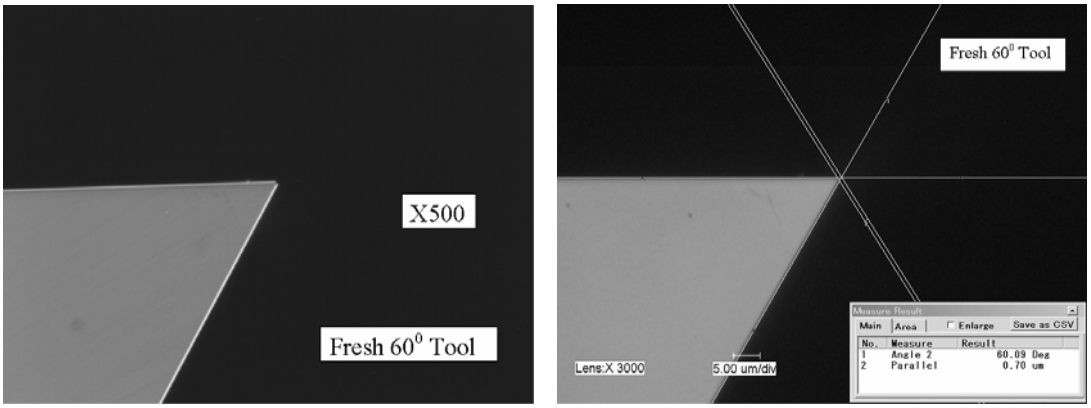

Figure-5.4(a) Figure-5.4(b)

Figure-5.4: Microscopic views of the rake face of a fresh 60^0 tool (tool-8); 5.4(a) - Nomarski image and 5.4(b) - Keyence image

The Nomarski and Keyence images of the left flank and right flank faces are shown in the figures 5.5 and 5.6. From figures 5.5a and 5.5b it could be seen that the left flank edge had fewer wear marks as compared to previous 45^0 tool (figure- 5.2). However some stain marks on the cutting edge of the rake face could be seen in the figure 5.5a. Figures 5.6 show that the right flank edge had more wear marks compared to the left flank edge (figure- 5.5), however fewer than the 45^0 one (figure- 5.3).

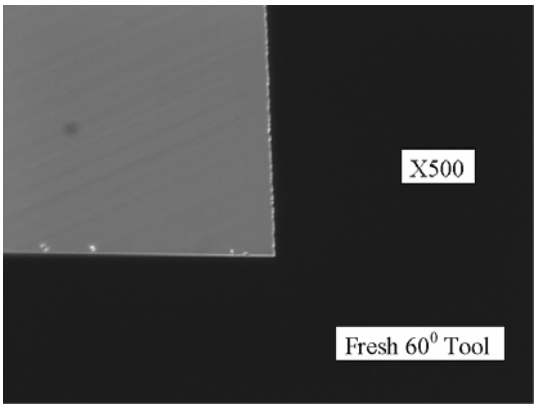

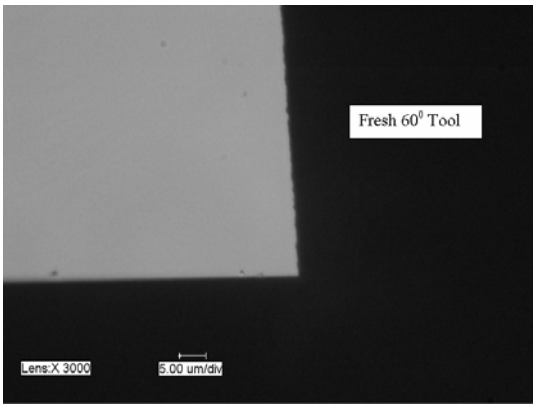

Figure-5.5(a) Figure-5.5(b)

Figure-5.5: Microscopic views of the left flank face of a fresh 60^0 tool (tool-8); 5.5(a) - Nomarski image and 5.5(b) - Keyence image

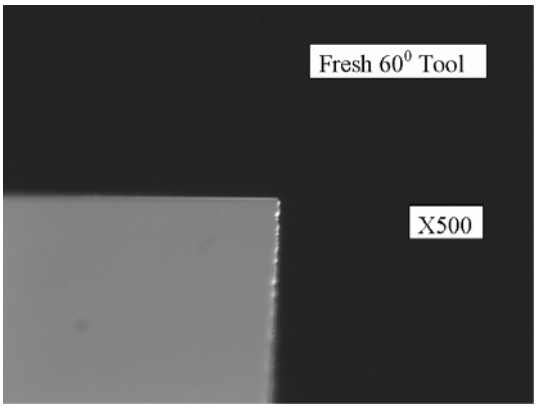

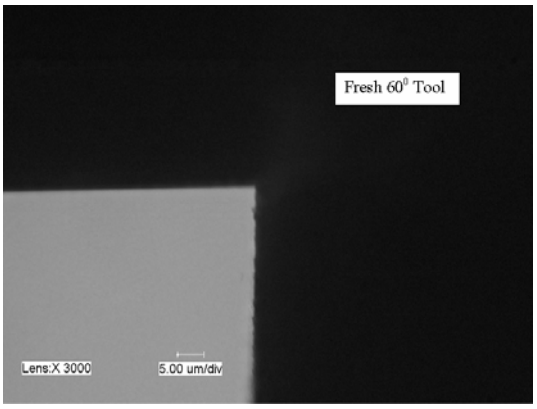

Figure-5.6(a) Figure-5.6(b)

Figure-5.6: Microscopic views of the right flank face of a fresh 60^0 tool (tool-8); 5.6(a) - Nomarski image and 5.6(b) - Keyence image

In this study each and every tool was checked in the similar fashion prior to the experiment. The initial wear marks could play a significant role on the tool life. The tools with severe initial wear marks on the flank edges failed in the very early stage of the experiment. In such cases the experiments were repeated with new tools until the satisfactory results were obtained. This wear marks also caused the chipping-off of the flank edge.

5.3 Effects of Cutting Parameters on Tool Life

Three cutting parameters were varied in this study to analyze the effects of the cutting parameters on the tool life. They are the infeed rate, the cutting speed and the lubricant material. Three different infeed rates, three different cutting speeds and two different lubricant materials were applied. With the same cutting combination two experiments were performed, one using 45^0 tool and another using 60^0 tool. Here the tool life was estimated based on 1.0μm wear of tool nose. The cutting distance was calculated based on complete groove cutting length.

5.3.1 Effect of Infeed Rate on Tool Life

In order to investigate the effect of infeed rate on tool life, the cutting speed was kept constant at 32.1m/min (= 100rpm of spindle speed) and UP2T lubricant was used. Three infeed rates of 0.5, 1.0 and 2.0μm/rev were used.

The tool wear progression is shown in the figure 5.7. Figure 5.7a shows the wear progression for 45^0 tools while figure 5.7b shows that for the 60^0 tools. Figure 5.7a shows that 45^0 tools experienced a catastrophic failure in each case; however for the 60^0 tool this occurred only when 1.0μm/rev infeed rate was used (figure 5.7b). For both types of the tools at 2.0μm/rev infeed rate, the tools faced the lowest wear progression, whereas at 0.5μm/rev they faced the highest wear progression and at 1.0μm/rev they faced a wear progression in between of 0.5 and 2.0μm/rev infeed rates.

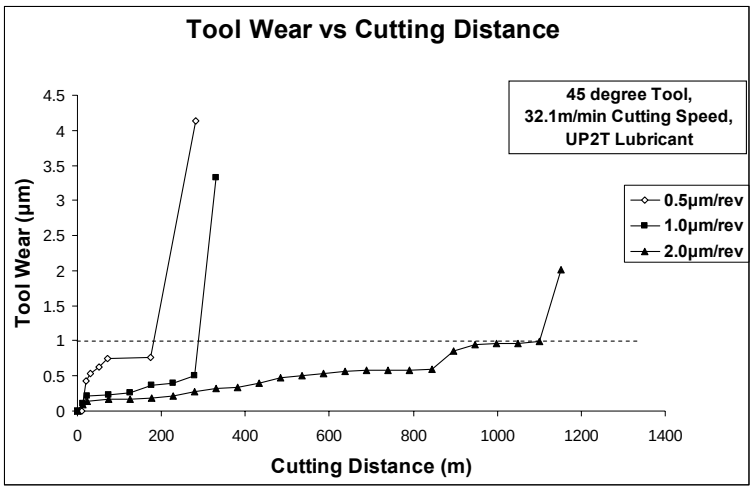

Figure-5.7(a): Effect of Infeed Rate on Tool Wear Progression for 45^0 Tools

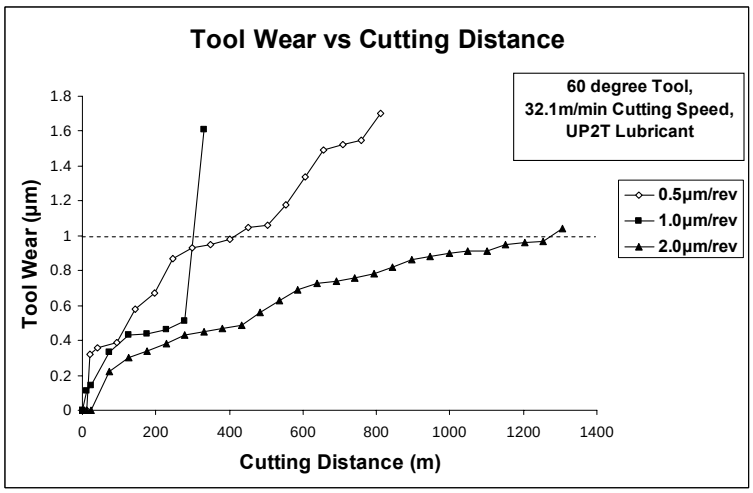

Figure-5.7(b): Effect of Infeed Rate on Tool Wear Progression for 60^0 Tools

The effects of the infeed rate on tool life are shown in figures 5.8a and 5.8b. From the experimental results, it was found that for higher infeed rate, the single crystal diamond tool can achieve higher tool life based on groove cutting distance. Moreover figures 5.8a and 5.8b show that for 2.0µm/rev infeed rate, both types of tools achieved significantly higher tool life based on groove cutting distance on tool failure at 1.0µm tool nose wear.

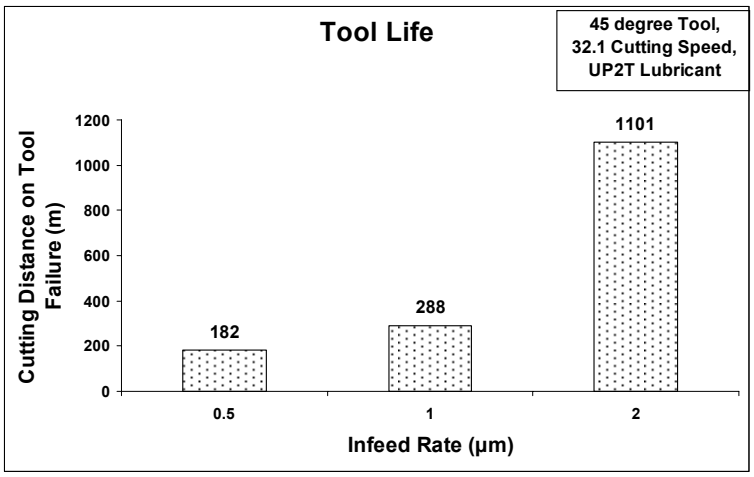

Figure-5.8(a): Effect of Infeed Rate on Tool Life for 45^0 Tools

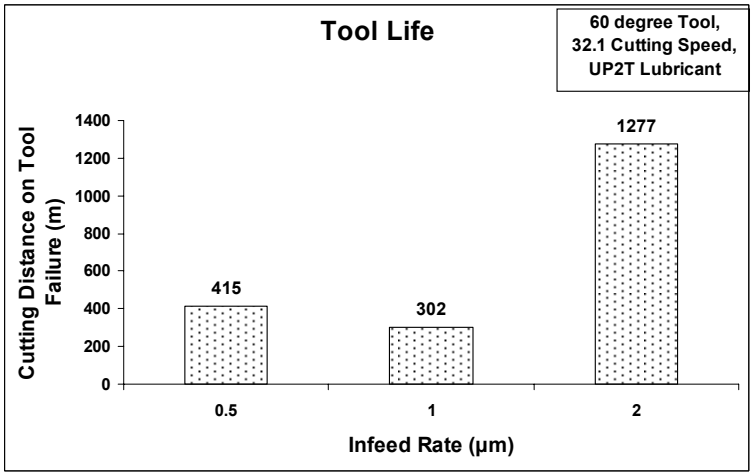

Figure-5.8(b): Effect of Infeed Rate on Tool Life for 60^0 Tools

For lower infeed rate (i.e. smaller depth of cut) the elastic recovery of the workpiece is higher and it pushes back the tool which enhances the tool wear. Moreover for lower infeed rate the loading on the tool is higher due to the fact that tool penetrates the workpiece with a smaller volume of tool tip. Because of this high stress on it the tool wears faster. For higher infeed rate (i.e. bigger depth of cut) due to the greater contact area the cutting face substantially shares the material removal process along with tool tip. However for lower infeed rate the tool point mainly removes the material and hence wears faster. In this study higher infeed rate also achieved higher tool life.

5.3.1.1 Effect of Infeed Rate on Tool Nose Wear

At some certain intervals the tools were checked under Nomarski and Keyence microscopes. After failure, the tools were checked under SEM. At each interval the tool nose wear was measured using the data processing unit of the Keyence microscope. For both types of tools gradual progression of the nose wear was observed at the initial stage of the machining. The 45^0 tools experienced the catastrophic failure for all three infeed rates, whereas the 60^0 tool experienced only once for the infeed rate of 1.0μm/rev. Figures 5.9 show the catastrophic failure of the tool nose for a 45^0 tool in the experiment 3. In figure 5.9b, it can be observed that there was a chip-off of tool nose measuring 9.20μm.

The SEM image of the same worn tool is shown in the figure 5.10. It shows the all three faces of the tool in one image. From the SEM image it could be seen that the catastrophic failure occurred along the flank edge and on the left flank. For all other catastrophic failure it was observed that failure initiated along the flank edge and finally the tool tip chipped off.

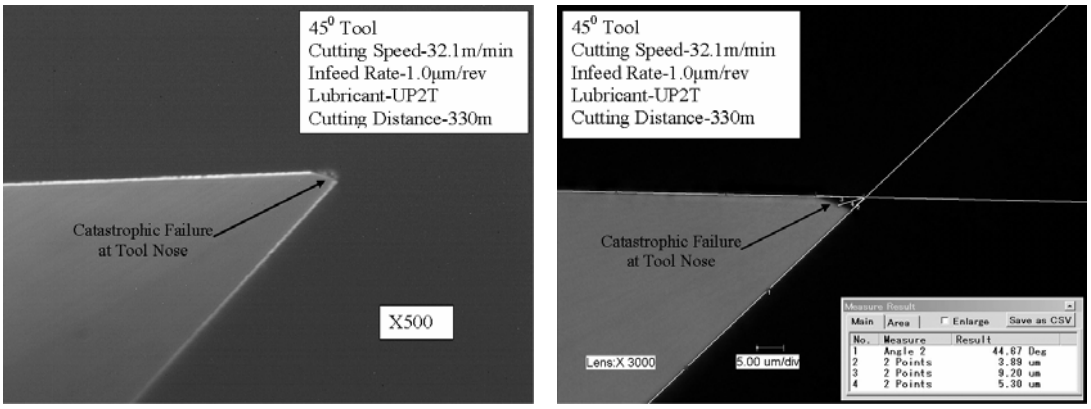

Figure-5.9(a) Figure-5.9(b)

Figure-5.9: Catastrophic failure of tool nose for a 45^0 tool (tool-3, rake face); 5.9a- Nomarski image and 5.9b- Keyence image

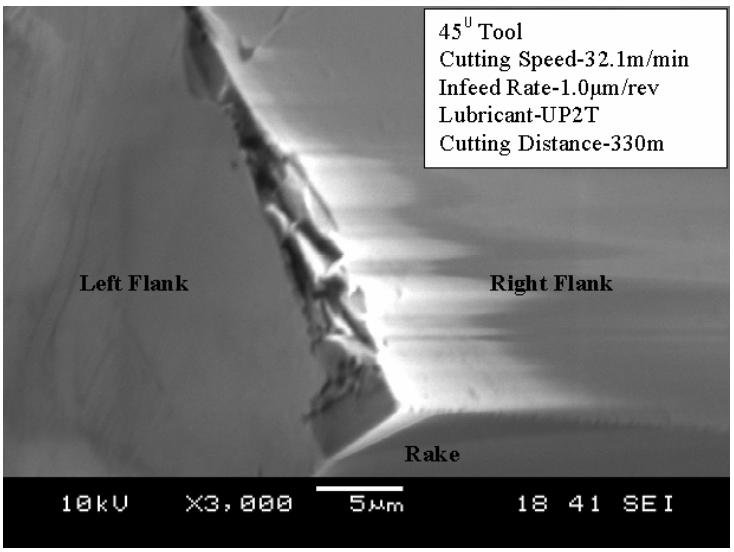

Figure-5.10: SEM image of catastrophic failure of a 45^0 tool (tool-3)

Two types of tool failure were observed in this set of experiments. The first one was the catastrophic failure and the other one was gradual progression of tool wear up to 1.0µm. Figures 5.11 show the gradual progression of tool wear for a 60^0 tool. The bigger included angle of 60^0 tools compared to that of 45^0 one made it stronger and more resistant to catastrophic failure. However for 1.0µm/rev infeed rate, the 60^0 tool also experienced a catastrophic failure. In the figure 5.11a the thick portion of the bright line near the tool tip shows gradual progression wear of the tool.

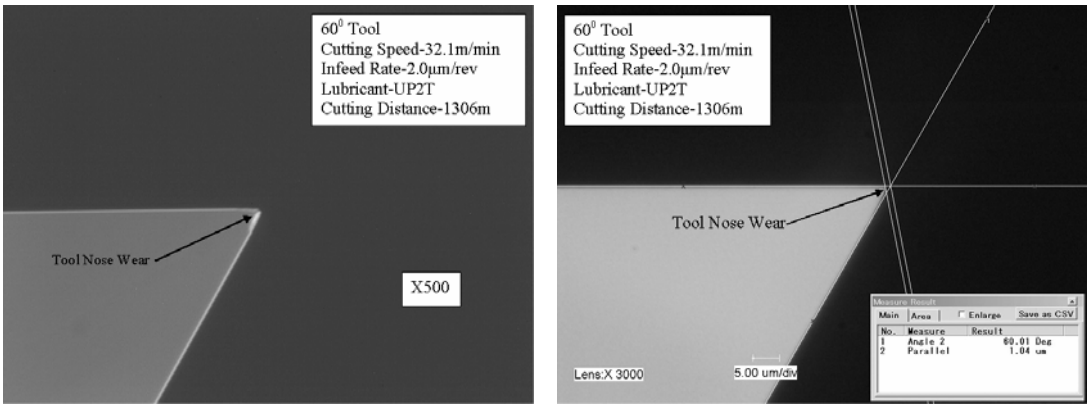

Figure-5.11(a) Figure-5.11(b)

Figure-5.11: Gradual progression of tool wear for a 60^0 tool (tool-14, rake face); 5.11a- Nomarski image and 5.11b- Keyence image

5.3.1.2 Effect of Infeed Rate on Cutting Force

The cutting force (F_c) and the thrust force (F_t) were recorded during the experiment. The cutting forces for the final pass of the machining are shown in the figures 5.12 and 5.13. From the figures 5.12a and 5.12b it can be observed that cutting force (F_c) increased faster due to the faster tool wear. The similar trend is observed in figures 5.13a and 5.13b for the thrust force (F_t). The lowest cutting force (F_c) and thrust force (F_t) justifies the highest tool life for the 2.0µm/rev infeed rate.

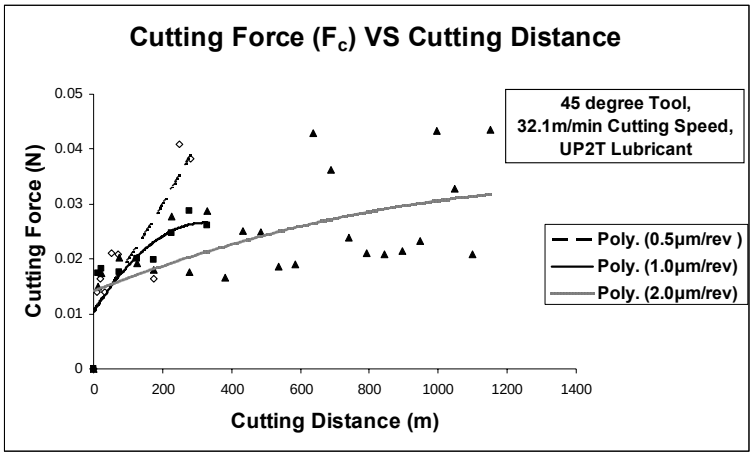

Figure-5.12(a): Effect of Infeed Rate on Cutting Force (F_c) for 45^0 Tools

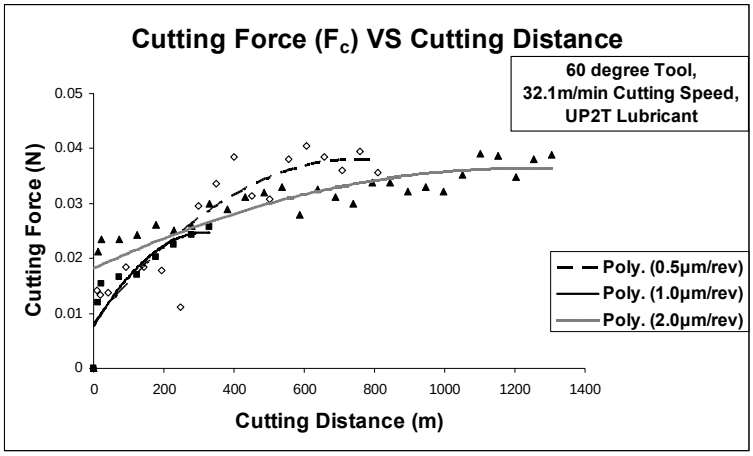

Figure-5.12(b): Effect of Infeed Rate on Cutting Force (F_c) for 60^0 Tools

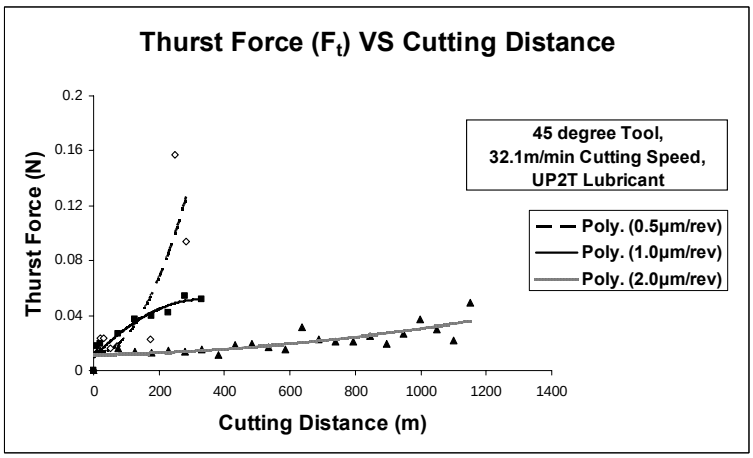

Figure-5.13(a): Effect of Infeed Rate on Thrust Force (F_t) for 45^0 Tools

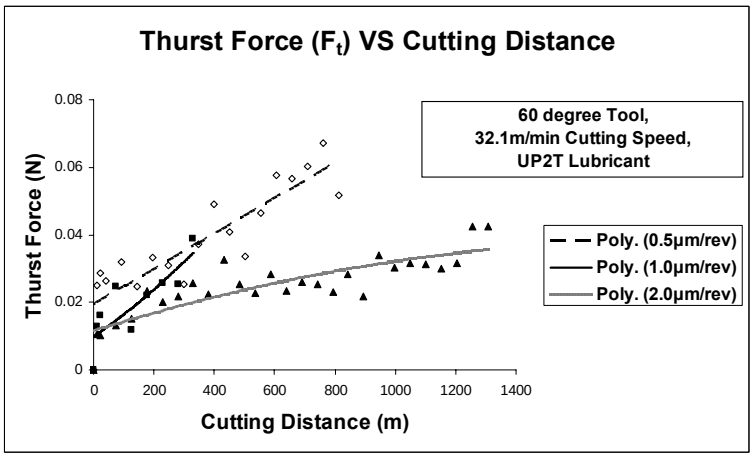

Figure-5.13(b): Effect of Infeed Rate on Thrust Force (F_t) for 60^0 Tools

Figures 5.14a and 5.14b show the effect of infeed rates on the F_c/F_t. The ratio of F_c/F_t less than 1.0 shows that thrust force (F_t) is dominating over the cutting force. For lower infeed rate due to the elastic recovery of the workpiece, there is push back effect on the tools, hence the thrust force increases over the cutting force. The values of the F_c/F_t for the 0.5µm/rev and 1.0µm/rev were found less than 1.0 (figures 5.14). Hence they justify the faster wear of tools for those infeed rate. However for 2.0µm/rev infeed rate the values of F_c/F_t were more than 1.0 except at the end of the machining when the tool was worn out (figures 5.14a and 5.14b). For worn tool, the thrust force is greater than the cutting force.

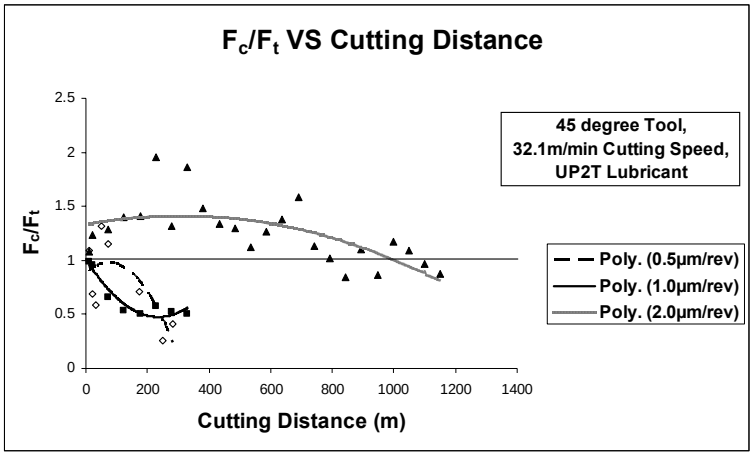

Figure-5.14(a): Effect of Infeed Rate on F_c/F_t for 45^0 Tools

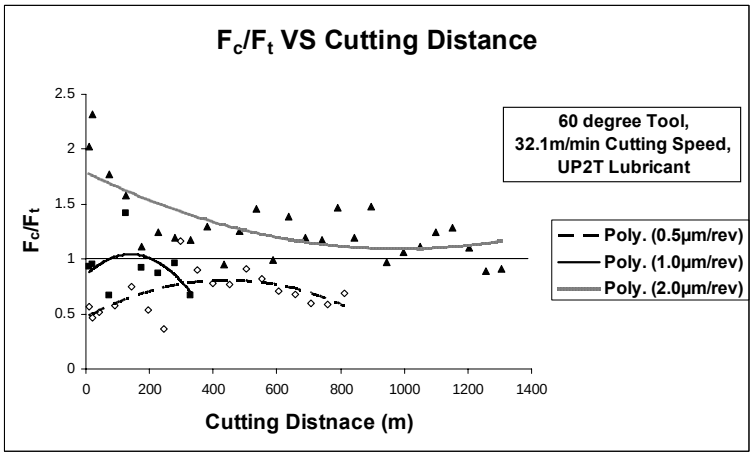

Figure-5.14(b): Effect of Infeed Rate on F_c/F_t for 60^0 Tools

5.3.2 Effect of Cutting Speed on Tool Life

In this set of experiments, infeed rate was kept constant at 1.0µm/rev and UP2T lubricant was used. Three cutting speeds of 9.6m/min (=30rpm), 19.2m/min (=60rpm) and 32.1m/min (=100rpm) were used. Each set of cutting parameters was tested with both the 45^0 and 60^0 tools.

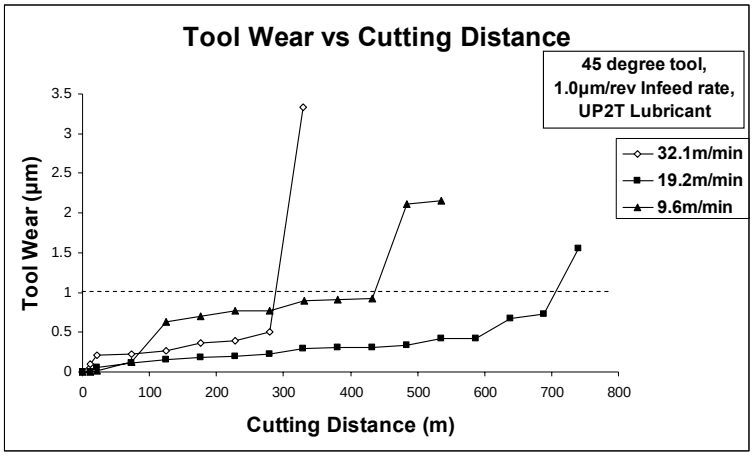

Figure-5.15(a): Effect of Cutting Speed on Tool Wear Progression for 45^0 Tools

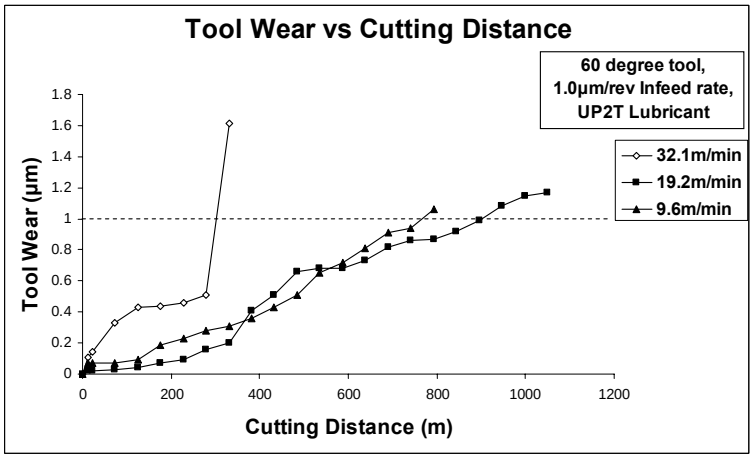

Figure-5.15(b): Effect of Cutting Speed on Tool Wear Progression for 60^0 Tools

Figures 5.15 show the effect of cutting speed on tool wear progression. It was found from this set of experiment that 45^0 tools experienced a catastrophic failure for all

three cutting speeds; however the 60^0 tool experienced that type of failure only when 32.1m/min cutting speed was used. For both types of tools the cutting speed of 19.2m/min achieved the lowest progression of the tool wear.

The effect of cutting speed on tool life is shown in the figures 5.16. The experimental results show that for a mid range cutting speed of 19.2m/min both types of cutter can achieve the longest tool life based on groove cutting distance on tool failure.

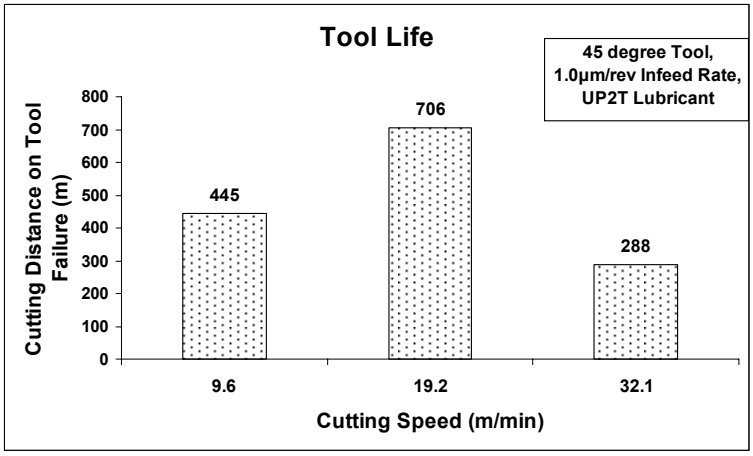

Figure-5.16(a): Effect of Cutting Speed on Tool Life for 45^0 Tools

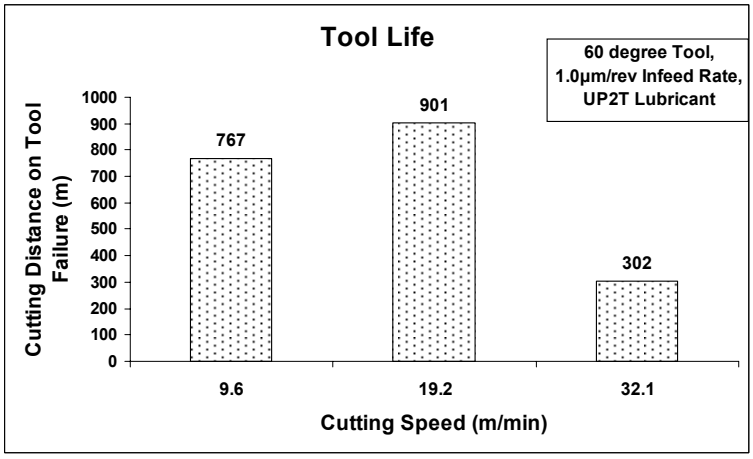

Figure-5.16(b): Effect of Cutting Speed on Tool Life for 60^0 Tools

For higher cutting speed the impact load on the tool tip is higher which accelerates the tool wear. Finally it leads to catastrophic failure of the tool tip. These phenomena can be seen from the figures 5.15a and 5.15b. However the lower cutting speed accelerates the flank wear. Severe wear marks on the flank edge were observed for 9.2m/min cutting speed for the both types of tools. These gradually weakened the tool tip and finally the tool tip failed. In this study it was found that at a cutting speed between 32.1m/min and 9.6m/min for both the tools achieved the longest tool life. The midrange value of 19.2m/min cutting speed attained this.

5.3.2.1 Effect of Cutting Speed on Tool Nose Wear

From the experimental results it was found that 45^0 tools experienced the catastrophic failure for all three cutting speeds, whereas 60^0 tool experienced only when the 32.1m/min cutting speed was used. Figures 5.17 and 5.18 represent the microscopic views of the rake face of a 45^0 and a 60^0 tool respectively. For the both cases the tool nose experienced catastrophic failure; however the breakage of tool nose was less compared to previous set of experiments (figure-5.9). A maximum breakage of tool nose of 3.68μm was observed for tool-5 (figure-5.17b). In figure 5.18b it can be seen that the tool nose breakage was up to 1.86μm. This small area of catastrophic failure proves that it was due to the impact loading on the tool tip for higher cutting speed of 32.1m/min.

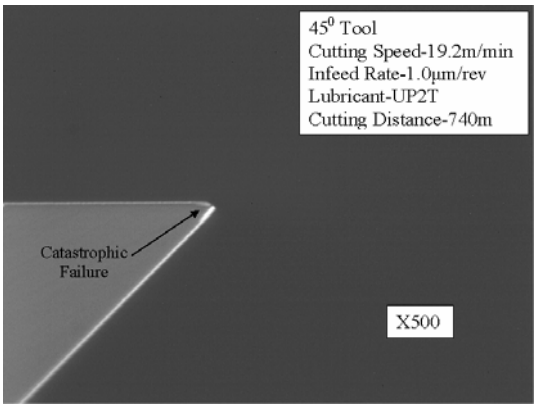

Figure-5.17(a)

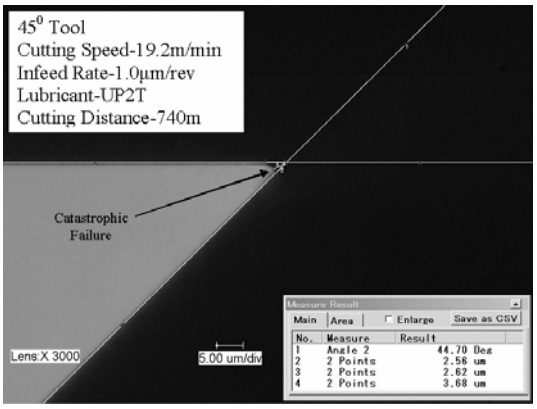

Figure-5.17(b)

Figure-5.17: Catastrophic failure of tool nose for a 45^0 tool (tool-5, rake face); 5.17a- Nomarski image and 5.17b- Keyence image

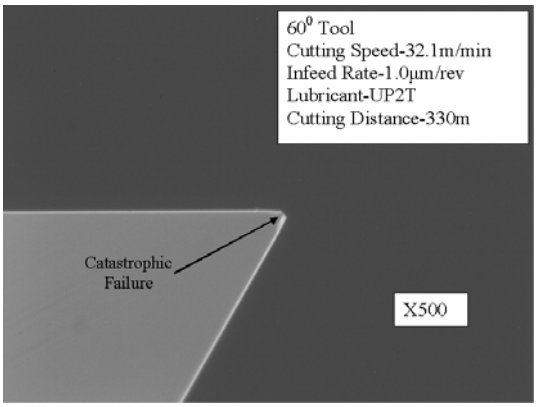

Figure-5.18(a)

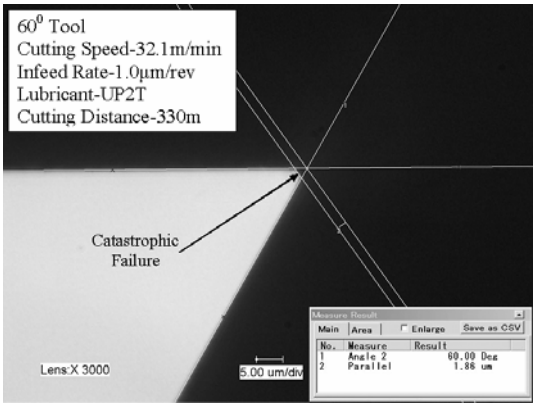

Figure-5.18(b)

Figure-5.18: Catastrophic failure of tool nose for a 60^0 tool (tool-13, rake face); 5.18a- Nomarski image and 5.18b- Keyence image

5.3.2.2 Effect of Cutting Speed on Cutting Force

The effects of cutting speeds on cutting force components are represented in the figures 5.19 and 5.20. Figure 5.19a shows that for 45^0 tools the cutting force (F_c) was the lowest for the highest cutting speed 32.1m/min. However for 60^0 tools after the initial stage of the machining cutting force (F_c) increased faster due to the tool wear. At higher cutting speed the cutting tool penetrates the workpiece faster, increases the temperature and thus softens the material. Hence the strain of the workpiece material

increases and finally the cutting force decreases. Similar trends can be seen for the thrust force (F_t) from the figures 5.20a and 5.20b. From the figures 5.21 it can be seen that the values of F_c/F_t are below 1.0, i.e. thrust force was dominating over the cutting force.

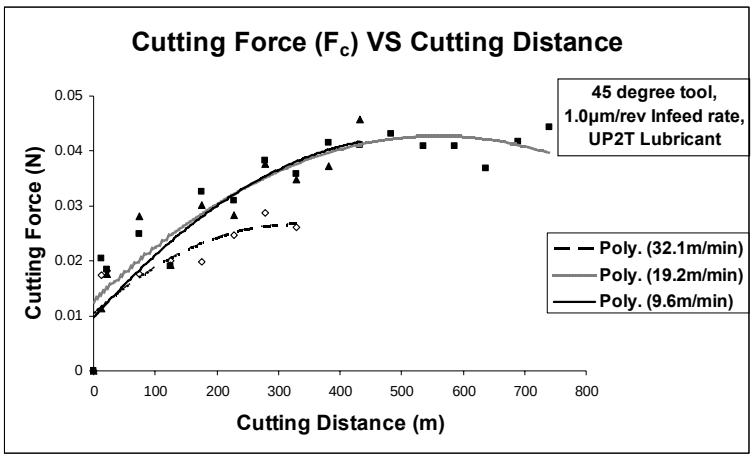

Figure-5.19(a): Effect of Cutting Speed on Cutting Force (F_c) for 45^0 Tools

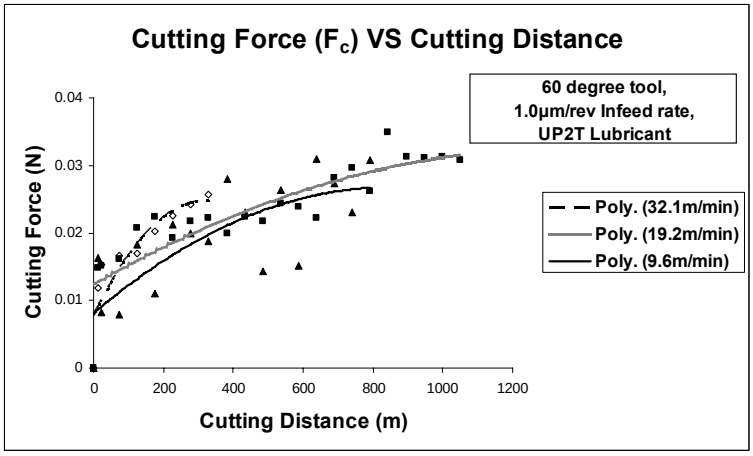

Figure-5.19(b): Effect of Cutting Speed on Cutting Force (F_c) for 60^0 Tools

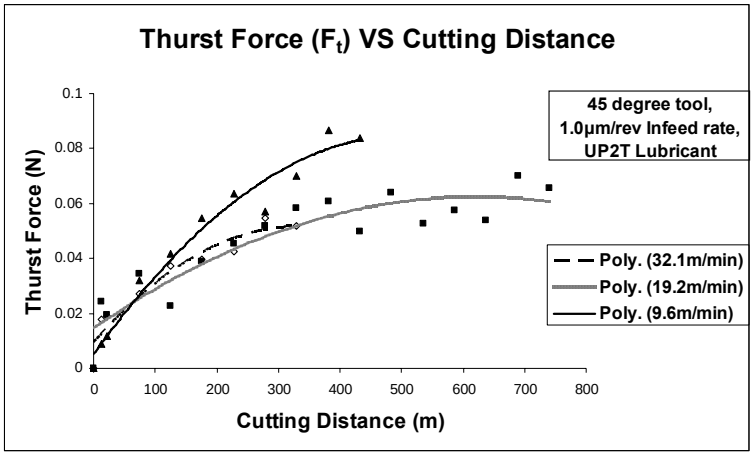

Figure 5.20(a): Effect of Cutting Speed on Thrust Force (F_t) for 45^0 Tools

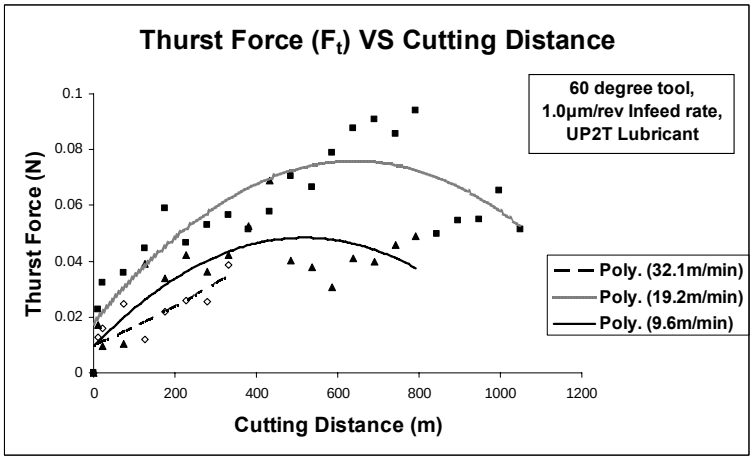

Figure-5.20(b): Effect of Cutting Speed on Thrust Force (F_t) for 60^0 Tools

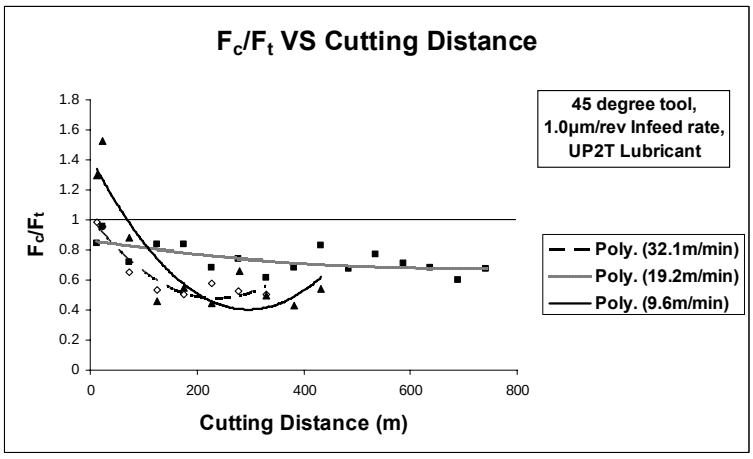

Figure 5.21(a): Effect of Cutting Speed on F_c/F_t for 45^0 Tools

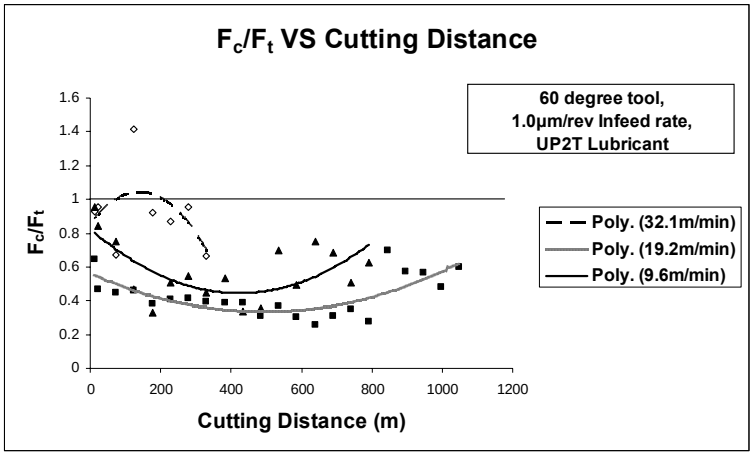

Figure-5.21(b): Effect of Cutting Speed on F_c/F_t for 60^0 Tools

5.3.3 Effect of Lubricant Material on Tool Life

In order to investigate the effect of lubricant material on tool life, the infeed rate and the cutting speed were kept constant at 1.0µm/rev and 19.2m/min respectively. Two lubricant material namely UP2T (a kerosene based mist) and vegetable oil (Johnson's Baby Oil) were used. The same cutting conditions were used for both 45^0 and 60^0 tools. The viscosity of the UP2T is less than that of vegetable oil and so it is able to penetrate to the cutting zone more easily. However being more volatile it may evaporate faster from the cutting zone than the vegetable oil and the vegetable oil may have more lubricating effect than the UP2T.

Figures 5.22a and 5.22b show the effect of lubricant material on tool wear progression. From figure 5.22a, it can be seen that the 45^0 tool failed catastrophically only when the UP2T lubricant was used. However for all the other cases in this set of experiments, both the 45^0 and 60^0 tools experienced gradual progression of tool wear beyond 1.0µm (figures 5.22a and 5.22b).

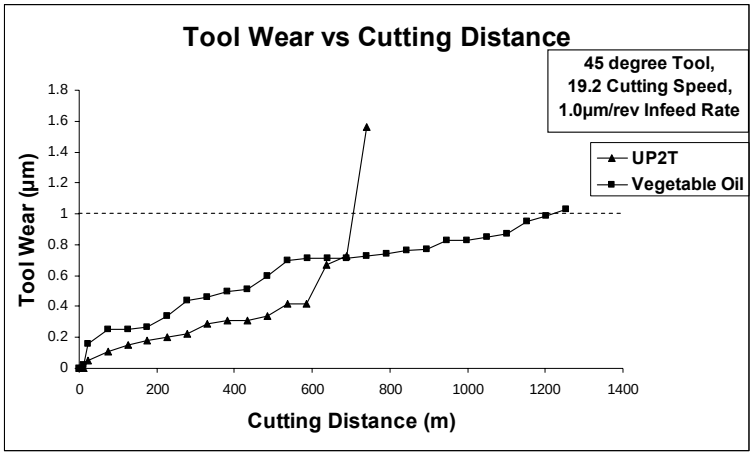

Figure-5.22(a): Effect of Lubricant Material on Tool Wear Progression for 45^0 tools

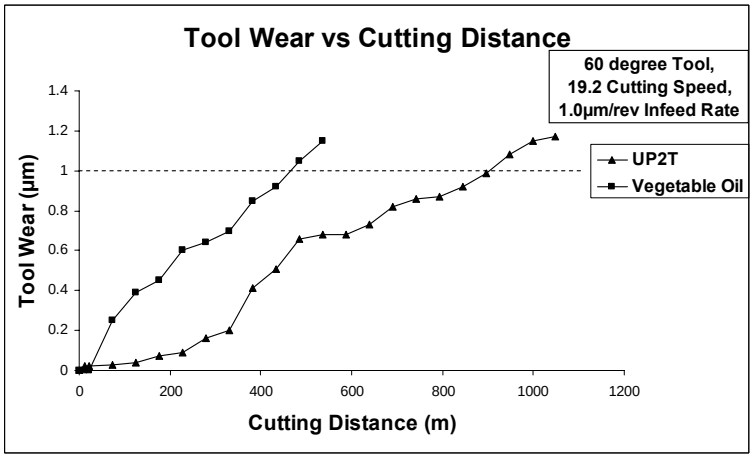

Figure-5.22(b): Effect of Lubricant Material on Tool Wear Progression for 60^0 tools

The effect of lubricant material on tool life is shown in the figures 5.23a and 5.23b. From the figure 5.23a it could be seen that the 45^0 tool achieved a significantly larger tool life for the vegetable oil lubricant. However the 60^0 tool achieved also a significantly longer tool life for the UP2T lubricant. From these contrasting results it is not possible to give a conclusive comment on choice of lubricant material.

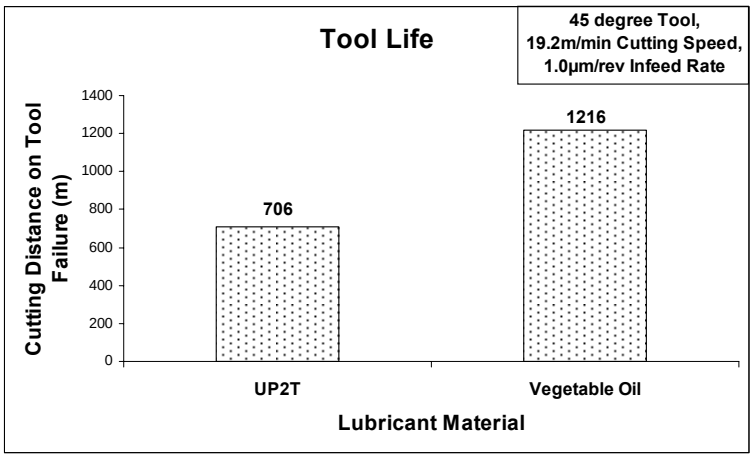

Figure-5.23(a): Effect of Lubricant Material on Tool Life for 45^0 Tools

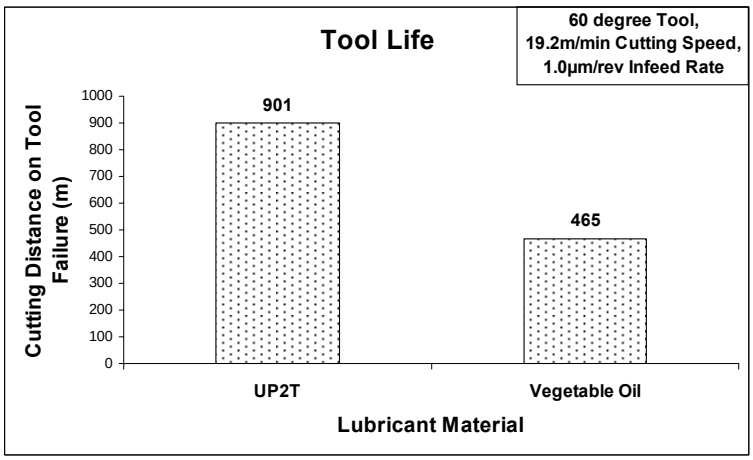

Figure-5.23(b): Effect of Lubricant Material on Tool Life for 60^0 Tools

5.3.3.1 Effect of Lubricant Material on Tool Nose Wear

The experimental results show that the 45^0 faced the catastrophic failure only when the UP2T lubricant was used. For other cases in this set of experiments both the tools wore gradually. Figures 5.24 and 5.25 represent the microscopic views of the rake face of a 45^0 and a 60^0 tool respectively. It could be seen from the figures 5.24 and 5.25 that both the tools wore gradually. The bright lines on the rake face show the waviness of the rake face of that tool (figure 5.25a).

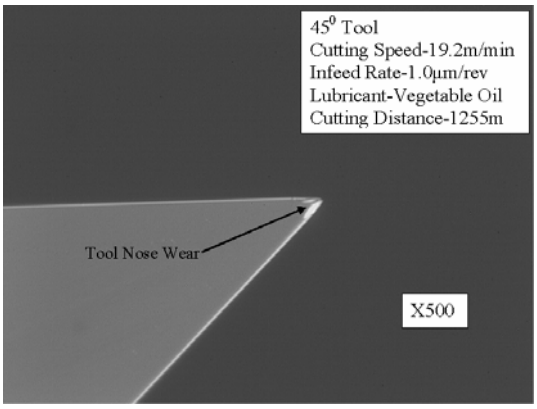

Figure-5.24(a)

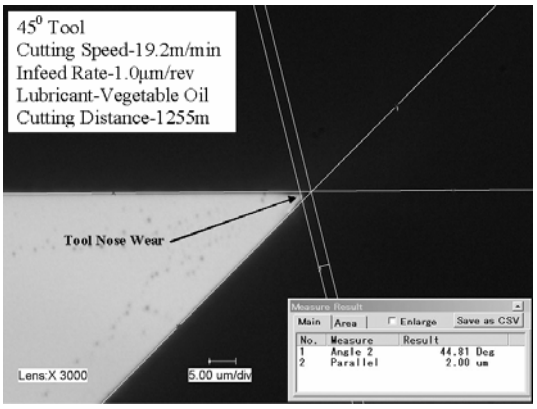

Figure-5.24(b)

Figure-5.24: Gradual progression of tool wear for a 45^0 tool (tool-11, rake face); 5.24a- Nomarski image and 5.24b- Keyence image

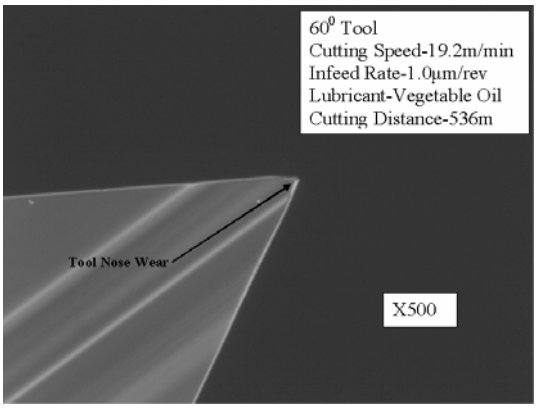

Figure-5.25(a)

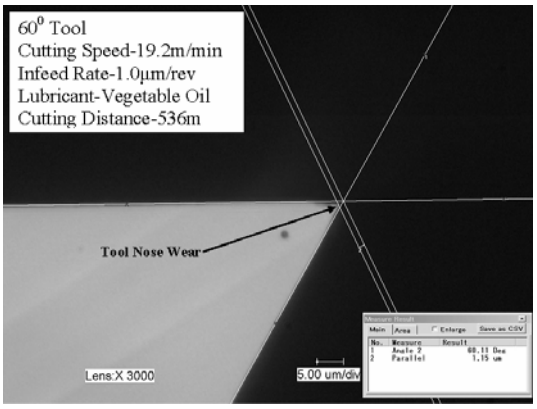

Figure-5.25(b)

Figure-5.25: Gradual progression of tool wear for a 60^0 tool (tool-15, rake face); 5.25a- Nomarski image and 5.25b- Keyence image

5.4 Performance Comparison between 45^0 and 60^0 Tools

In this study single crystal diamond tools with two tool point angles of 45^0 and 60^0 were used. For each set of cutting parameters (infeed rate, cutting speed and lubricant material), two experiments were conducted with these two types of tools. The performance comparisons between these tools were performed based on the tool life achieved for that particular set of cutting parameters. For most cases, the 45^0 tools experienced catastrophic failures while the 60^0 tools mostly wore gradually.

Figure 5.26 shows the performance comparison between 45^0 and 60^0 tools for the variation of the infeed rate. For this a constant cutting speed of 32.1m/min and UP2T lubricant were used. Three different infeed rates of 0.5μm/rev, 1.0μm/rev and 2.0μm/rev were used. From the figure 5.26 it could be seen that 60^0 tools achieved lomger tool life for every set of cutting parameters.

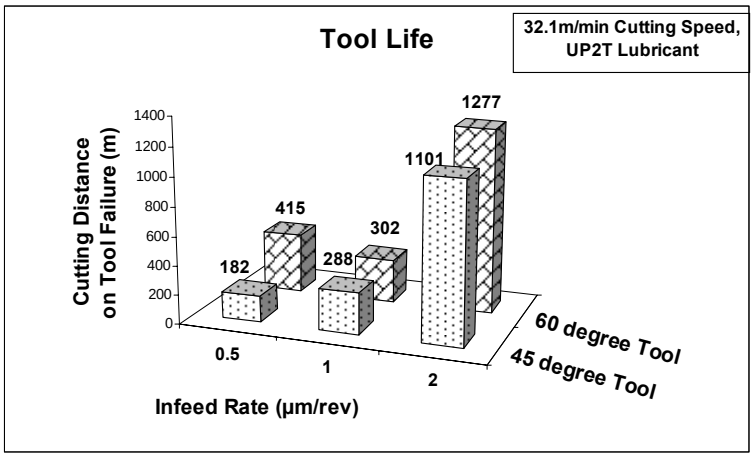

Figure-5.26: Performance Comparison between 45^0 and 60^0 Tools
(Variation of Infeed Rate)

The performance comparison between 45^0 and 60^0 tools for the variation of the cutting speeds is shown in the figure 5.27. In order to do that the infeed rate was kept constant at 1.0μm/rev and UP2T lubricant was used. Three cutting speeds of 9.6m/min, 19.2m/min and 32.1m/min were applied. For this set of experiments 60^0 tools show the better tool life.

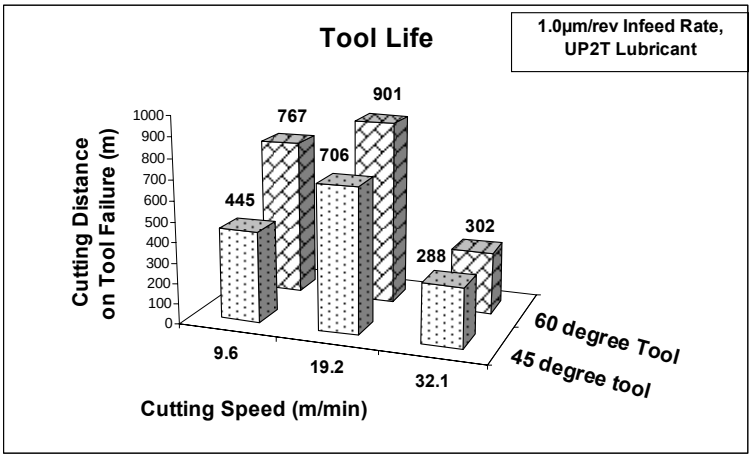

Figure-5.27: Performance Comparison between 45^0 and 60^0 Tools
(Variation of Cutting speed)

Figure 5.28 shows the performance comparison between 45^0 and 60^0 tools for the variation of the lubricant material. The infeed rate and cutting speed were constant at 1.0μm/rev and 19.2m/min respectively. Two lubricant materials namely UP2T and vegetable oil were applied. The experimental results show that 60^0 tool achieved higher tool life for UP2T lubricant, whereas 45^0 tool achieved higher tool life for vegetable oil lubricant (figure-5.28). From these contradictory results it is not possible to comment on the performance of the diamond tools for the variation of lubricant materials.

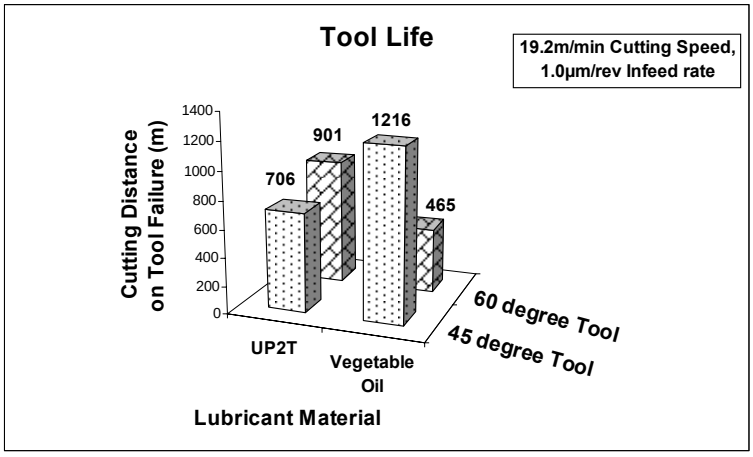

Figure-5.28: Performance Comparison between 45^0 and 60^0 Tools
(Variation of Lubricant Material)

5.5 Flank Wear

In this study, flank wear played a very significant role in tool wear and it was found that the flank edge wore much faster than the cutting edges. For several cases it was found that there was no mark of tool wear on the cutting edges and tool nose on the rake face, but the flank edge experienced substantial wear. Several grooves were observed on the flank face from the early stage of the machining (figure 5.29a). As the machining continued, the microgrooves increased on the flank face covering a larger area (figure 5.29b). Once it has covered a significant area then the tool either failed gradually or in some cases tool failed catastrophically. Figures 5.30a and 5.30b show the left flank face of a 45^0 tool after two different cutting distances and this tool experienced a catastrophic failure on its nose.

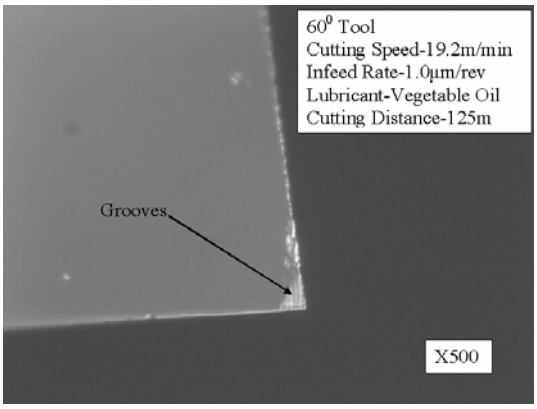

Figure-5.29(a)

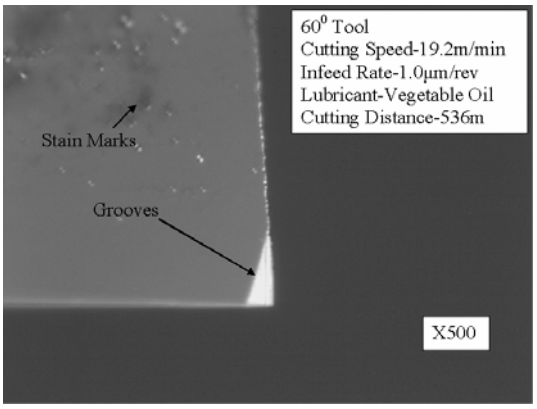

Figure-5.29(b)

Figure-5.29: Nomarski image of grooves on left flank face of a 60^0 tool (tool-15); 5.29a- after 125m and 5.29b- after 536m cutting distance

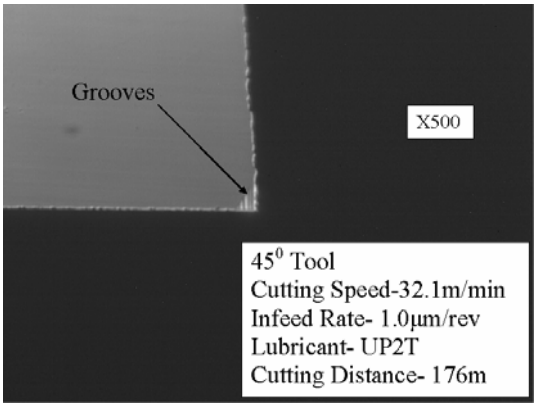

Figure-5.30(a)

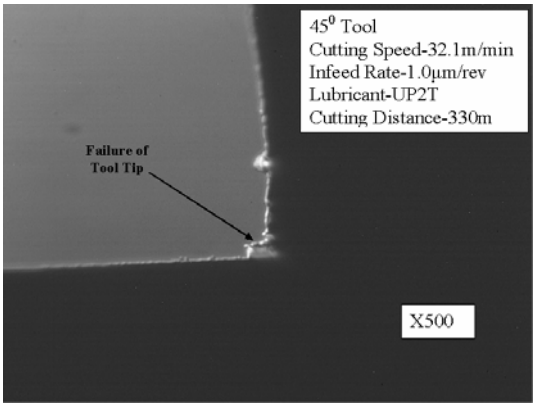

Figure-5.30(b)

Figure-5.30: Nomarski image of grooves on left flank face of a 45^0 tool (tool-3); 5.30a- after 176m and 5.30b- after 330m cutting distance

Figure 5.31 show the Keyence microscope image of the left flank face of a 45^0 tool after a cutting distance of 279m. A SEM image of a 45^0 tool is shown in the figure 5.32. From this image the three faces of the tool can be seen. Both the left and right flank faces had distinct grooves.

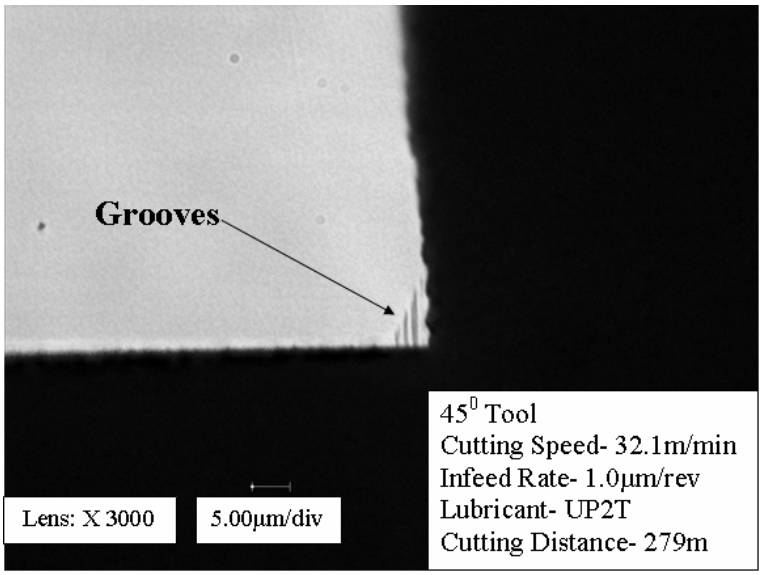

Figure-5.31: Keyence image of grooves on left flank face of a 45^0 tool (tool-3), after 279m cutting distance

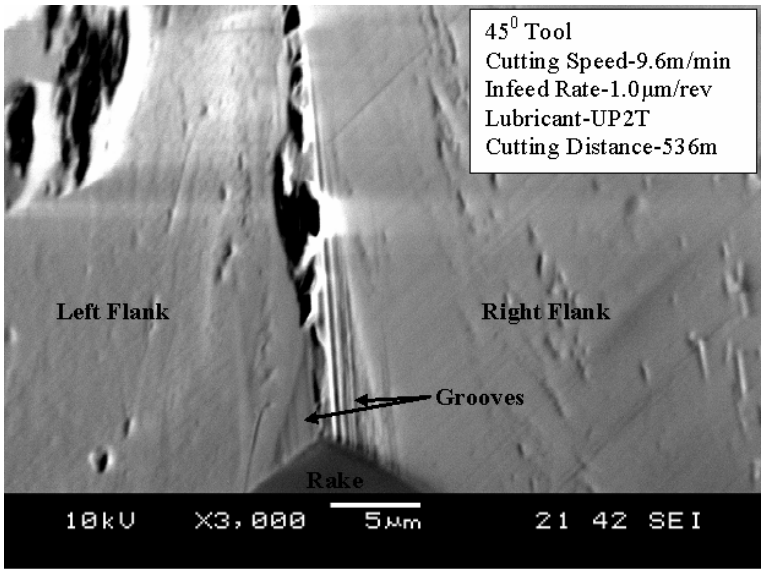

Figure-5.32: SEM image of a 45^0 tool (tool-9) after 536m cutting distance

Some chipped-off areas at a distant away from the cutting zone on the flank face were observed before reaching the wear criterion. These might be caused by some sub-surface cracks of the tools. Moreover as these tools were made of artificial diamond, they might have some impurities and the area on the impurity chipped off due to the force and vibration transmitted from the cutting zone. Figure 5.33 shows a chipped-off area of 137.92μm^2 and 18.03μm from the tool tip. This is very far from the cutting zone and appeared after only cutting of 92m distance. However it remained the same until the tool failed. Figure 5.34 shows the SEM image of the same tool after a cutting distance of 811m and it confirms that the chipped-off area remained the same.

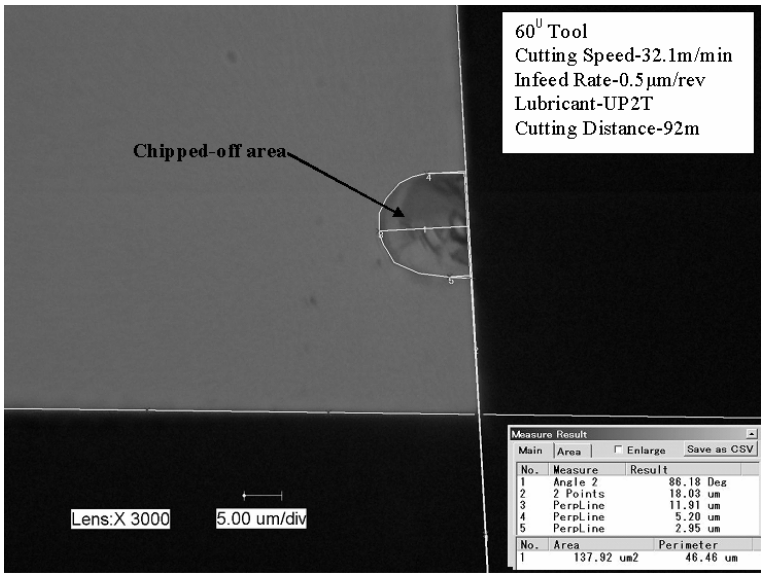

Figure-5.33: Keyence image of chipped-off area on left flank face of a 60^0 tool (tool-2), after 92m cutting distance

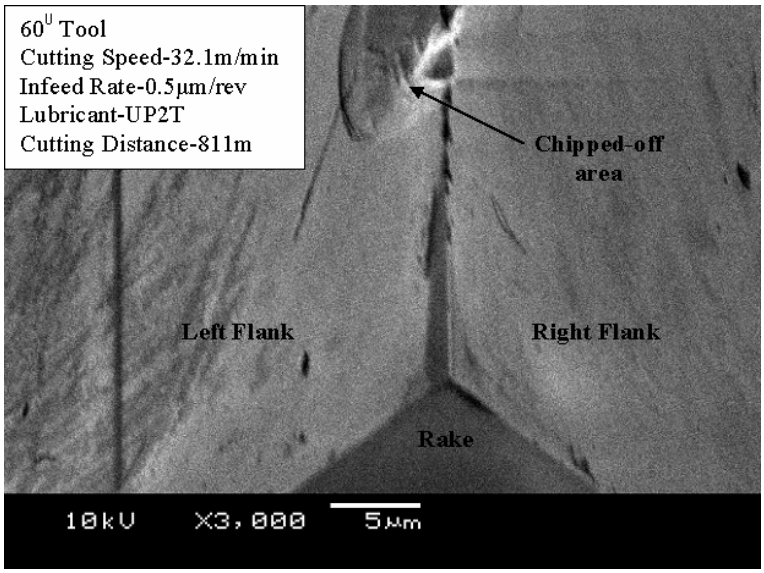

Figure-5.34: SEM image of a 60^0 tool (tool-2) after 811m cutting distance

Another chipped-off area observed after a cutting distance of 484m for a 60^0 tool (experiment-8). In this case it occurred in the cutting zone and also extended beyond the cutting zone. Figures 5.35a and 5.35b show the right and left flank faces of that tool indicating the chipped-off area. Due to this type of chipped-off area in the cutting zone the tool became weak and hence very prone to a catastrophic failure.

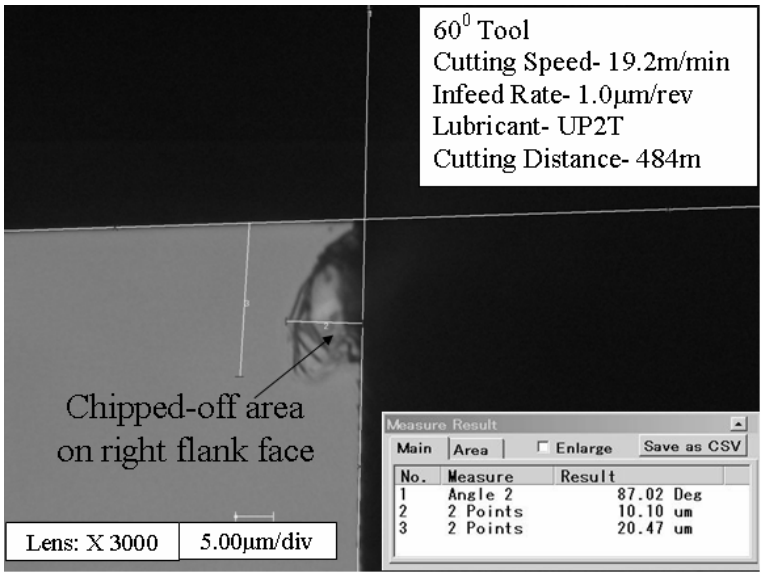

Figure-5.35(a): Keyence image of chipped-off area on right flank face of a 60^0 tool (tool-8), after 484m cutting distance

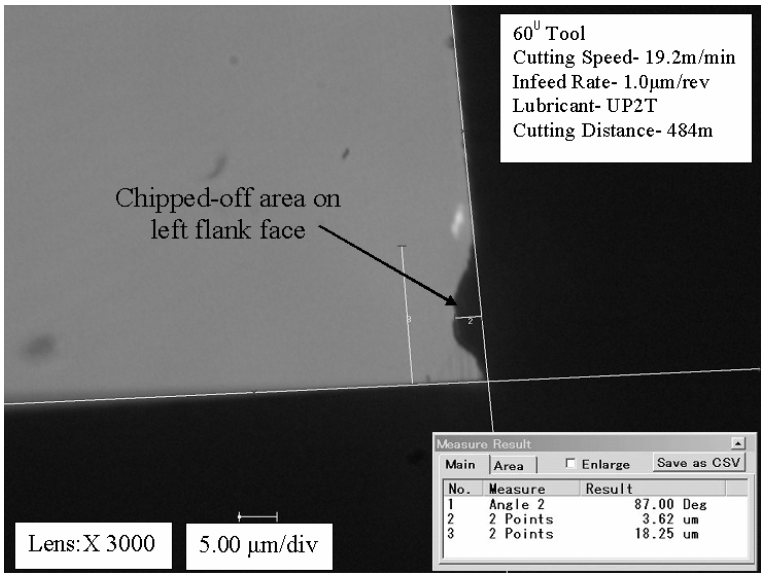

Figure-5.35(b): Keyence image of chipped-off area on left flank face of a 60^0 tool (tool-8), after 484m cutting distance

5.6 Machined Surface Observation

The observation of the machined surface was a destructive process. The workpiece was sawed into small slices to place on the work-table of the Keyence microscope. The workpiece machined in the experiment-10 was used for the observation. In this experiment a 60^0 tool was used to generate the grooves of 60^0 included angles. A cutting speed of 9.6m/min, infeed rate of 1.0µm/rev and UP2T lubricant were used in this experiment. The Nomarski microscope produced the 2-dimensional view of that machined surface (figure-5.36). The Keyence microscope can show both the 2-dimensional and 3-dimensional views of the machined surface. Figure 5.37 shows the 2-D Keyence image of the same surface. The 3-D Keyence image is shown in the figure 5.38. As the grooves were of only 5µm depth and of very narrow included angles of 45^0 and 60^0, it was not possible to measure the surface finish of the walls of grooves.

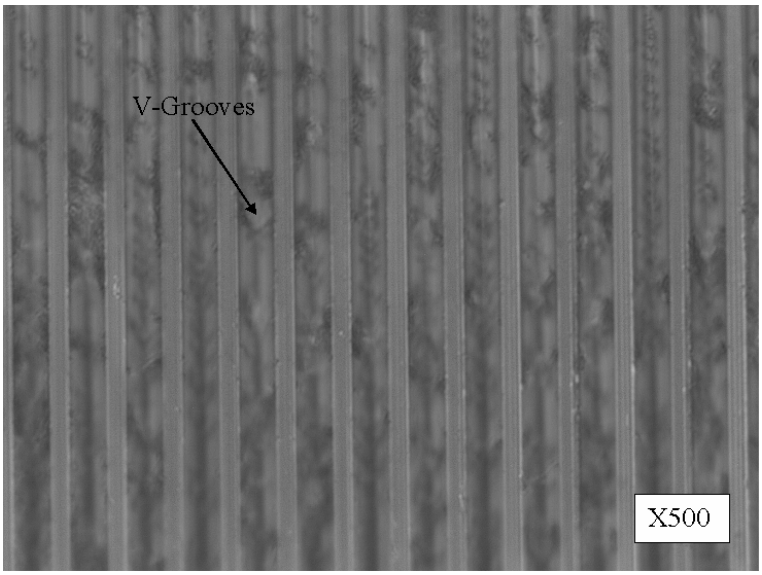

Figure-5.36: Nomarski image of Machined Surface

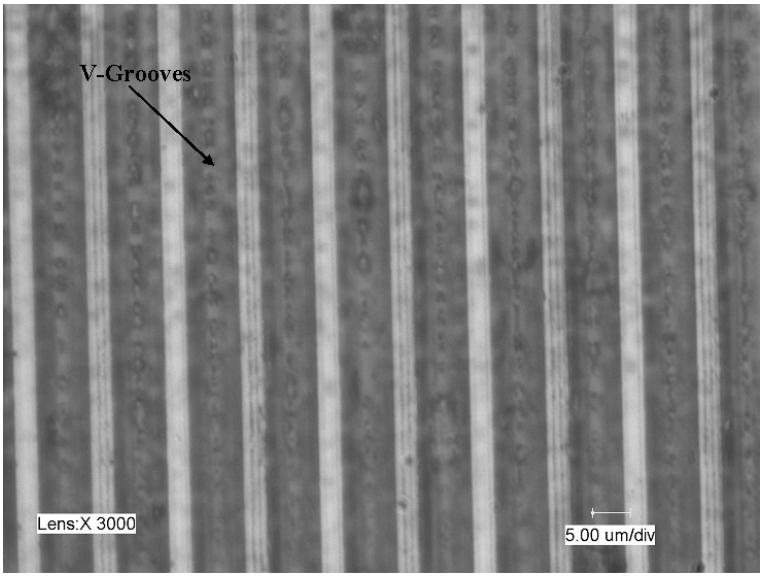

Figure-5.37: 2-Dimensional Keyence image of Machined Surface

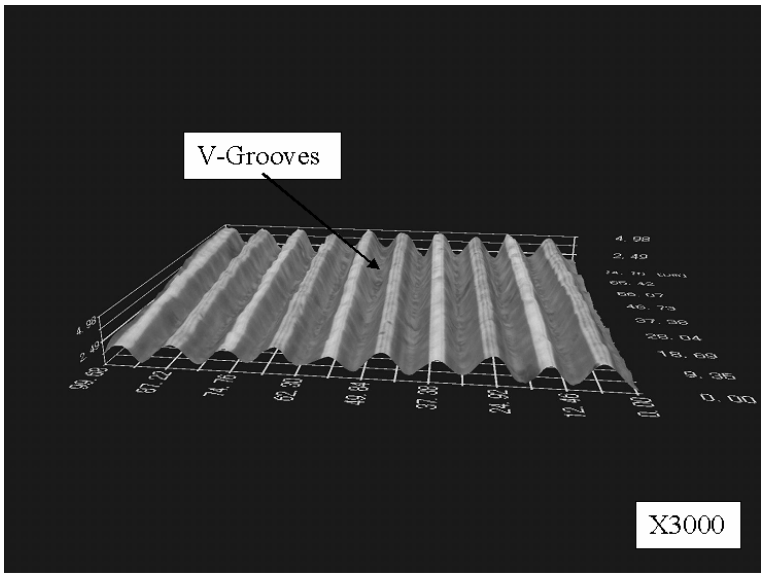

Figure-5.38: 3-Dimensional Keyence image of Machined Surface

5.7 Chips Observation

The cutting chips were collected during the machining and observed under SEM. Figures 5.39 to 5.42 show the cutting chips in a variety of magnification collected at different stage of machining in the experiment-4. For this experiment a 45^0 tool was used with the cutting speed of 32.1m/min, infeed rate of 2.0μm/rev and UP2T lubricant. From the figures it is evident that the cutting chips were continuous and wedge shaped which is consistent with the machining of the V-shapes of the grooves. Moreover it ensures the ductile mode machining of electroless nickel.

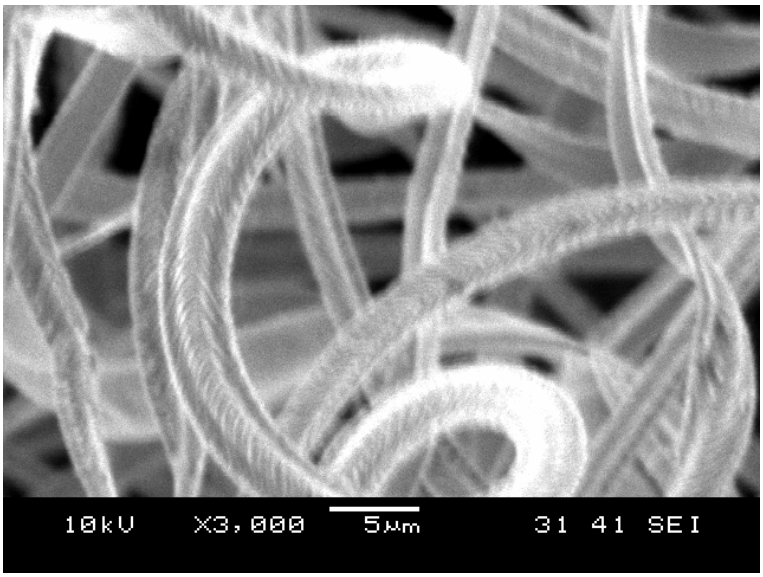

Figure-5.39: SEM image of the cutting chips in machining of 1.6m to 11.9m cutting distance (X3000)

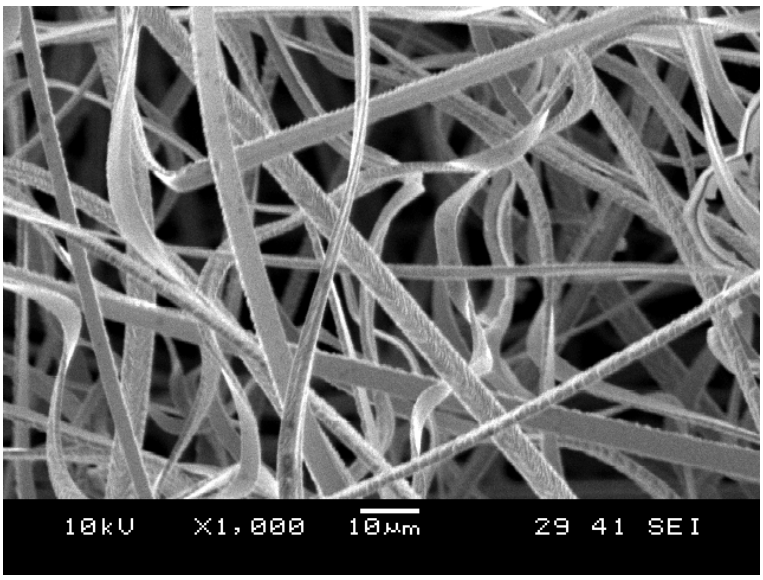

Figure-5.40: SEM image of the cutting chips in machining of 73.4m to 124.8m cutting distance (X1000)

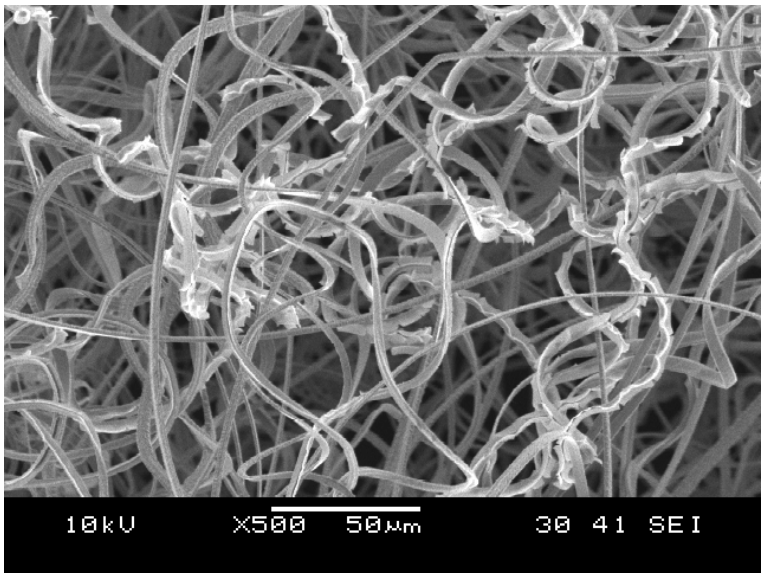

Figure-5.41: SEM image of the cutting chips in machining of 124.8m to 176.1m cutting distance (X500)

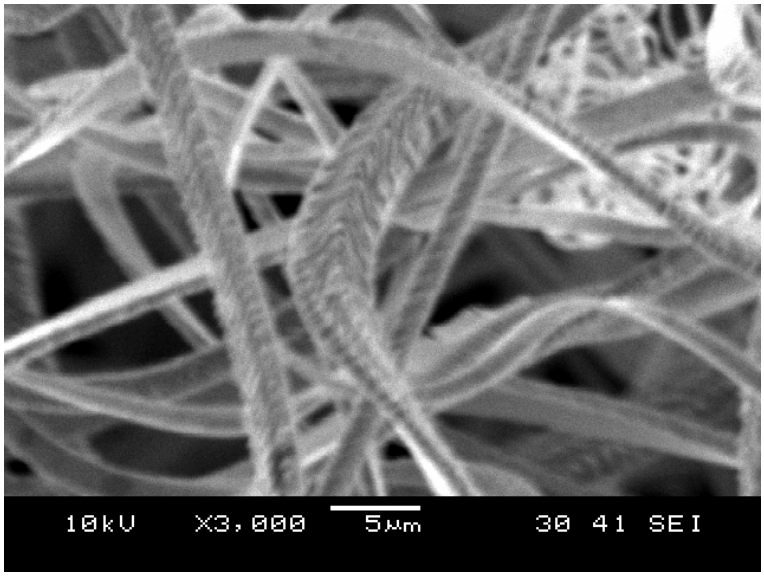

Figure-5.42: SEM image of the cutting chips in machining of 124.8m to 176.1m cutting distance (X3000)

5.8 Conclusions

The machining performances of single crystal diamond tools with tool point angles of 45^0 and 60^0 for micro-cutting of V-grooves on cylindrical workpiece of electroless nickel plated die materials have been studied. The experimental results show that 2.0μm/rev infeed rate and 19.2m/min cutting speed lead to the higher tool life based on groove cutting distance. However no conclusive result has been found for selecting the lubricant material. It has been also observed that the 60^0 tool can achieve higher tool life compared to the 45^0 tool.

Chapter Six: Conclusions and Recommendations

6.1 Introduction

The main purpose of this study was to evaluate the effects of the cutting parameters on tool life of single crystal diamond tools with different tool point angles in machining V-shape micro-grooves of narrow included angles of 45^0 and 60^0 on the Electroless Nickel Plated cylindrical dies. In conjunction with the effects on tool life, the wear characteristics of diamond tools were analyzed. Finally the performances of 45^0 and 60^0 tools were compared. In addition the machined surface and the cutting chips were observed. In this study the tool life was estimated based on 1.0μm wear of the tool nose and interpreted in terms of cutting distance. The cutting distance was calculated based on the complete groove cutting length. Three cutting parameters namely the infeed rate, the cutting speed and the lubricant material were varied. The intent of this chapter is to present the concluding remarks from this study and also to make recommendations for the future work.

6.2 Conclusions

The following conclusions are drawn from this study.

- From the investigation on the effects of infeed rate, it was found that the tool life increased with the increasing infeed rate for the both types of tools and at 2.0μm/rev infeed rate they can achieve the longest tool life.
- Experimental results show that at a mid range cutting speed of 19.2m/min both the 45^0 and 60^0 tools can achieve the longest tool life.

- From the experimental results it was found that the 45^0 tool achieved higher tool life with vegetable oil whereas the 60^0 tool achieved higher tool life with UP2T. However from this contrasting result no conclusive remark could make on the choice of the lubricant material.
- The 45^0 tools experienced a catastrophic failure of tool nose in the most cases whereas the 60^0 tools failed only once catastrophically. However until the tools failed they wore gradually with the cutting distance.
- The microscopic observations of the tools during the experiments reveal that there were increasing micro-grooves at the cutting zone on the flank faces with increasing cutting distance and finally caused the tools to fail. Moreover chippings from the flank edge were observed during the machining.
- In the early stage of the machining several chipped-off areas were observed at a distance away the cutting zone and they remained unchanged for rest of the experiment.
- From the experimental results it is obtained that the 60^0 performed better in terms of tool life than the 45^0 tools except the case where vegetable oil lubricant was used. In that case the 45^0 tool achieved higher tool life than the 60^0 tool.
- The cutting chips observation confirms the production of continuous and wedge shape chips as well as the V-shapes of the grooves and hence ductile mode machining.

6.3 Recommendations

The followings are the recommendation made for the future work.

- In order to obtain a conclusive result for the investigation of the effects of the lubricant material on the tool life, four more experiments should be done by changing the cutting speed and the infeed rate.
- It would be very interesting to repeat the whole set of experiments with the Ultra Precision Cutter (abbreviated in UPC) to verify the results. However the tool cost would be five times higher for UPC tools.
- The natural diamond could be introduced in place of artificial one as cutting tool to achieve longer tool life.
- The online observation of the cutting tools could be applied. This would reduce the experiment time in a significant amount.
- Due to the size limitation of the Keyence microscope, the machined surface observation was a destructive process. This could be avoided if the necessary changes in the structure of Keyence Microscope are made. Moreover highly sophisticated Optical Surface Profiler could be employed to check the surface finish of the machined grooves.
- The cutting chips analysis would be very interesting if a high resolution SEM is used for the observation.
- A cutting force model in relation to the diamond tool wear in micro-grooving on electroless nickel plated dies should be developed.

Bibliography

Asai, S. and A. Kobayashi. Observations of Chip Producing Behavior in Ultra-Precision Diamond Machining and Study on Mirror-like Surface Generating Mechanism, Precision Engineering, 12, pp. 137-143. 1990.

Baudrand, D. W. Metals Hand Book. Ohio: American Society for Metals. 1978.

Bhattacharyya, A. Metal Cutting Theory and Practice. pp. 126, Calcutta: New Central Book Agency. 1984.

Biddut, A. Q. Micro-Grooving on Electroless Nickel Plated Die Materials. M.Eng. Thesis, National University of Singapore. 2005

Blackley, W. S. and R. O. Scattergood. Chip Topography for Ductile Regime Machining of Germanium, Journal of Engineering for Industry, 116, pp.263-266. 1994.

Boothroyd, Geoffrey and Winston A. Knight. Fundamentals of Machining and Machine Tools. pp. 82, New York: Marcel Dekker. 1989.

Casstevens, J. M. and C. E. Daugherty. Diamond Turning of Optical Surface on Electroless Nickel, Precision Machining of Optics, 159, pp. 109-113. 1978.

Davis, J. R. and Davis & Associates (ed). ASM Specialty Handbook: Nickel, Cobalt, and Their Alloys. pp. 114-118, USA: ASM International. 2000.

Dini, J. W. Electroless Nickel – An Important Coating for Diamond Turning Applications. In Proc. Electroless Nickel Conference II, 1981, Cincinnati, Ohio, USA.

Duncan, R. N. Effect of Solution Age on Corrosion Resistance of EN Plating, Surface Finishing, 83, pp. 64-68. 1983.

Fang, F. Z. and V. C. Venkatesh. Diamond Cutting of Silicon with Nanometric Fininsh, Annals of the CIRP, 47, pp. 45-49. 1998.

Ikawa, N., R. R. Donaldson, R. Kumanduri, W. Konog, P. A. Mckeown and I. F. Stowers. Ultra Precision Metal Cutting – The Past, the Present and the Future, Annals of the CIRP, 40, pp. 587-594. 1991.

Ikawa, N., S. Shimada and H. Morooka. Technology of Diamond Tool for Ultra Precision Metal Cutting, Bulletin: Japan Society of Precision Engineering, 21, pp. 233-238. 1987.

Komanduri, R., N. Chandrasekaran and L. M. Raff. Effects of Tools Geometry on Nanometric Cutting: A Molecular Dynamics Simulation Approach, Wear, 219, pp. 84-97. 1998.

Li, X. P., M. Rahman, K. Liu, K. S. Neo and C. C. Chan. Nano-precision Measurement of Diamond Tool Edge Radius for Wafer Fabrication, Journal of Materials Processing Technology, 140, pp. 358-362. 2003.

Mallory, Glenn O. and Juan B. Hajdu (ed). Electroless Plating: Fundamentals and Applications. pp. 115-135. Orlando, Florida: American Electroplaters and Surface Finishers' Society. 1990.

Moriwaki, T., E. Shamoto and K. Inoue. Ultra Precision Ductile Cutting of Glass by Applying Ultrasonic Vibration, Annals of the CIRP, 41, pp. 141-144. 1992.

Moriwaki, T., H. Akira and O. Koichi. Effect of Cutting Heat on Machining Accuracy in Ultra-precision Diamond Turning, Annals of the CIRP, 39, pp. 81-85, 1990.

Oomen, J. M. and J. Eisses. Wear of Monocrystalline Diamond Tools During Ultra Precision Machining of Nonferrous Metals, Precision Engineering, 14, pp. 206-218. 1992.

Park, S. H. and D. N. Lee. Study on the Microstructure and Phase Transformation of Electroless Nickel Deposits, Journal of Material Science, 23, pp. 1643-1654. 1988.

Parker, K. Recent Advances in Electroless Nickel Deposits. In Proc. 8th International Conference, September 1972, Basel, Switzerland, pp. 202-207.

Pramanik, A. Ultra-Precision Machining of Electroless Nickel Plated Die Materials. M.Eng. Thesis, National University of Singapore. 2004.

Pramanik, A., K. S. Neo, M. Rahman, X. P. Li, M. Sawa and Y. Maeda. Cutting Performance of Diamond Tools During Ultra-Precision Turning of Electroless Nickel Plated Die Materials, Journal of Material Processing Technology, 140, pp. 308-313. 2003.

Rahman, K. M. Rezaur, M. Rahman, K. S. Neo, M. Sawa and Y. Maeda. Microgrooving on Electroless Nickel Plated Materials using A Single Crystal Diamond Tool, Int J Adv Manuf Technol, 27, pp. 911-917. 2006.

Reidel, Wolfgang. Electroless-Nickel Plating. pp. 206, Ohio: ASM International. 1991.

Sanger, G. M. and J. W. Dini. A Perspective on Electrodeposited and Electroless Nickel Coatings used in Optical Applications. In Proc. Surface Finish Conference, 1982, USA.

Son, S. M., H. S. Lim and J. H. Ahn. Effect of the Friction Coefficient on the Minimum Cutting Thickness in Micro Cutting, Int J Machine Tools & Manuf, 45, pp. 529-535. 2005.

Syn, C. K., J. S. Taylor and R. R. Donaldson. Diamond Tool Wear vs Cutting Distance on Electroless Nickel Mirrors, SPIE, 676, pp. 128-140. 1986.

Syn, C. K., J. W. Dini, J. S. Taylor, G. L. Mara, R. R. Vandervoort and R. R. Donaldson. Influence of Phosphorus Content and Heat Treatments on the Machinability of Electroless Nickel Deposits, In Proc. Electroless Nickel Conference IV, 1985, Chicago, Illinois, USA. pp. 5.1-5.15.

Taylor, J. S., C. K. Syn, T. T. Satio and R. R. Donaldson. Surface Finish Measurement of Diamond-turned Electroless-Nickel-Plated Mirrors, In Proc. SPIE's 29th Annual Technical Symposium, 1985, San Diego, USA.

Toh, S. B. and R. McPherson. Fine Scale Abrasive Wear of Ceramics by a Plastic Cutting Process, In Science of Hard materials, ed by E. A. Almond, C. A. Brookes and R. Warren, pp. 865-871, Bristol and Boston: Adam Hilger Ltd. 1986.

Trent, E. M. and Paul K. Wright. Metal Cutting. pp. 62-74, USA: Butterworth-Heinemann. 2000.

List of Publication

Conference Paper

Ghosh, A., K. S. Neo, T. Yoshikawa, C. H. Tan and M. Rahman. Performance Evaluation of Diamond Tools for Micro Cutting of V-Grooves on Electroless Nickel Plated Die Materials, In Proc. 7th euspen International Conference, May 2007, Bremen, Germany, vol I, pp. 135-138.